Increasing Stemness Drives Prostate Cancer Progression, Plasticity, Therapy Resistance and Poor Patient Survival

Xiaozhuo Liu[1§*], Eduardo Cortes[2,3§], Yibing Ji[1], Kathy Zhao[4], Julian Ho[4], Yang (Seagle) Liu[4], Elai Davicioni[4], Felix Y. Feng[5†], Joshi J. Alumkal[6], Daniel E. Spratt[7], Christopher J. Sweeney[8], Han Yu[2], Qiang Hu[2], Zou Cheng[9], Dingxiao Zhang[9], Gurkamal Chatta[10], Kent L. Nastiuk[11], David W. Goodrich[1], Kiera Rycaj[1], Anmbreen Jamroze[1], Jason S. Kirk[1], Igor Puzanov[10], Song Liu[2*], Jianmin Wang[2*], Dean G. Tang[1*]

[1]Department of Pharmacology and Therapeutics, Roswell Park Comprehensive Cancer Center, Buffalo, New York, USA
[2]Department of Biostatistics and Bioinformatics, Roswell Park Comprehensive Cancer Center, Buffalo, New York, USA
[3]Department of Biostatistics, University at Buffalo, Buffalo, New York, USA
[4]Veracyte Inc, San Diego, California, USA
[5]Department of Radiation Oncology, University of California, San Francisco, California, USA
[6]Department of Hematology and Oncology, Department of Internal Medicine, Rogel Cancer Center, University of Michigan, Ann Arbor, Michigan, USA
[7]University Hospitals Seidman Cancer Center and Case Western Reserve University, Cleveland, Ohio, USA
[8]South Australian Immunogenomics Cancer Institute, University of Adelaide, Adelaide, SA 5000, Australia
[9]School of Biomedical Sciences, Hunan University, Changsha, China
[10]Department of Medicine, Roswell Park Comprehensive Cancer Center, Buffalo, New York, USA
[11]Department of Cancer Genetics, Roswell Park Comprehensive Cancer Center, Buffalo, New York, USA

[§]These authors contributed equally to this work.

[†]We dedicate this work to the memory of Dr. Felix Y. Feng, whose contributions to this project and the field of prostate cancer research are immeasurable.

***Corresponding authors:**
Xiaozhuo Liu, PhD, Department of Pharmacology and Therapeutics, Roswell Park Comprehensive Cancer Center, Buffalo, NY 14263 (Phone: 716-645-4988, Xiaozhuo.Liu@Roswellpark.org).

Song Liu, PhD, Department of Biostatistics and Bioinformatics, Roswell Park Comprehensive Cancer Center, Buffalo, NY 14263 (Song.Liu@Roswellpark.org).

Jianmin Wang, PhD, Department of Biostatistics and Bioinformatics, Roswell Park Comprehensive Cancer Center, Buffalo, NY 14263 (Jianmin.Wang@Roswellpark.org).

Dean Tang, MD, PhD, Department of Pharmacology and Therapeutics, Roswell Park Comprehensive Cancer Center, Buffalo, NY 14263 (Dean.Tang@Roswellpark.org).

Conflict of interest: The authors declare no potential conflicts of interest.

Running title: Increasing Stemness Drives Prostate Cancer Progression.

Key words: Prostate cancer, stemness, AR signaling, aggressiveness, heterogeneity, plasticity.

Word counts: Main Text: 4786 words; Figures: 7; Supplementary Figures: 10; Supplementary Tables: 5.

ABSTRACT

Cancer development and progression are associated with loss of differentiation and gain of stem cell traits (stemness). Here, we test the hypothesis that in prostate cancer (PCa), the stemness level, assessed by a Stemness score metric, can quantitatively track PCa development and progression, therapy resistance, metastasis, and survival. Analysis of transcriptomic data from 3,102 RNA-seq and 84,081 microarray samples across 26 datasets reveals continually increasing Stemness and decreasing pro-differentiation androgen receptor activity (AR-A) along the PCa progression spectrum, with metastatic castration-resistant PCa (mCRPC) exhibiting the highest Stemness and lowest AR-A. Both the general Stemness score and a newly developed 12-gene 'PCa-Stem Signature' correlate with and predict poor patient survival. We also present evidence that elevated AR-A may drive increased Stemness in early-stage PCa, but key genomic alterations such as MYC amplification and bi-allelic RB1 loss likely drive greatly elevated Stemness in advanced, therapy-resistant and metastatic PCa where AR-A is suppressed.

STATEMENT OF SIGNIFICANCE

Here we adapt and develop Stemness-based metrics and signatures to assess tumor progression in the PCa continuum. Our results suggest that increased Stemness quantitatively measures PCa aggressiveness, plasticity and progression, and represents a poor prognosticator for patient outcomes.

INTRODUCTION

Malignant transformation and cancer progression are characterized by progressive loss of differentiation (or oncogenic dedifferentiation) and gain of stem cell traits (i.e., stemness), and poorly differentiated tumors are enriched in gene expression profiles of normal embryonic and adult stem cells and in cancer stem cells (1-5). However, the oncogenic dedifferentiation-based stemness concept (6) that prostate cancer (PCa) represents abnormal organogenesis (7, 8) is not currently addressed and there lack quantitative measurements of the overall stemness-associated aggressiveness in PCa.

PCa is projected to claim the lives of >35,000 American men in 2025 (9). PCa incidence rates increased 3% per year from 2014 - 2019 driven by advanced PCa diagnosis and the proportion of men diagnosed with metastases has doubled from 2011 to 2019 when the next generation of androgen receptor (AR) pathway inhibitors (ARPIs) such as abiraterone (Zytiga; FDA approval in 2011) and enzalutamide (Xtandi; FDA approval in 2012) were introduced to the clinic. Significant increases in aggressive disease and continued high PCa mortality have been linked to intrinsic PCa cell heterogeneity (e.g., in AR expression) and treatment-induced plasticity (8).

The level of malignancy of primary PCa (Pri-PCa) has been traditionally assessed by pathologists using a combined Gleason Score (GS), which gauges histopathological differentiation pattern of prostatic glands. The higher the GS, the more undifferentiated and more malignant the Pri-PCa is. The GS system, although clinically the ‘gold’ standard in pinpointing PCa diagnosis, is only semi-quantitative, can be subjective (to individual pathologist’s assessment), and is generally not applicable to treatment-failed tumors and distant metastases (which have mostly lost differentiated glandular structures). Notably, whether more advanced Pri-PCa (GS8-10), treatment failure and metastatic dissemination are quantitatively associated with increased cancer stemness remains unknown. On the other hand, AR is the master regulator of normal prostatic epithelium differentiation and represents the therapeutic target of PCa treatments including androgen-deprivation therapy (ADT) and ARPIs. Inevitably, tumors develop resistance to ADT/ARPIs leading to the state of castration-resistant PCa (CRPC), which involves many mechanisms including genetic alterations of *AR* and key genes in AR pathway (10), lineage plasticity (8,11,12), and increased stemness (8,13). It is unclear how the global pro-differentiation AR signaling activity changes and evolves during the spectrum of PCa initiation and progression and during development of treatment resistance and metastasis. These discussions raise the need to quantify the AR signaling and stemness and closely track their dynamic evolution and inter-relationship during PCa progression.

Herein, we adapted and developed transcriptome-based gene signature scores to quantitatively assess the pro-differentiation (canonical) AR activity (AR-A) and oncogenic stemness levels (Stemness Index or

Score) and their inter-relationship in the PCa spectrum. Specifically, we used gene expression data collected from 3,102 RNA-seq and 84,081 microarray samples in 26 distinct cohorts encompassing the PCa continuum, i.e., from normal/benign prostate to early stage, advanced and metastatic PCa, to pre- and post-therapy PCa, and, finally, mCRPC, to track the dynamic evolution of and inter-relationship between AR-A and the Stemness Index. Our results indicate that increased Stemness quantitatively tracks PCa aggressiveness, plasticity, treatment resistance and progression, and represents a poor prognostic factor for patient outcomes.

96 **RESULTS**
97

98 **Adapting and developing Stemness and AR-A metrics for PCa analysis.**
99 To determine the global and dynamic changes of and inter-relationship between degree of malignancy
100 (oncogenic dedifferentiation) and level of (luminal) differentiation during PCa development and progression
101 (Supplementary Fig. S1A-B), we employed two transcriptome-based algorithms to annotate 26 datasets
102 of 3,102 bulk RNA-seq and 84,081 microarray samples encompassing the PCa continuum (Supplementary
103 Fig. S1B; Supplementary Table S1). In our studies, we focused on and compared three progressive stages:
104 from normal prostate to localized Pri-PCa, from low-grade to high-grade Pri-PCa, and from treatment-naïve
105 Pri-PCa to CRPC/mCRPC (Supplementary Fig. S1A). We defined "progression" as stages beyond Pri-
106 PCa and as disease entities that are more aggressive in a comparative manner. Specifically, we adapted
107 the Stemness Index (6) (mRNAsi; **Stemness** for short) (Supplementary Fig. S1C) to gauge the degree of
108 malignancy (or aggressiveness) and employed the Z-score normalized canonical (pro-differentiation) AR
109 activity or **AR-A** (Supplementary Fig. S1D) to measure the level of differentiation. Canonical AR-A can be
110 determined by quantifying AR-regulated transcripts under intact androgen/AR signaling conditions, and
111 there are several such AR-regulated gene lists (14-18) (Supplementary Fig. S2A-B). We validated the AR-
112 A list based on their enrichment in prostatic epithelium differentiation, correlation of individual gene
113 expression with AR-A signatures in clinical datasets, and overall consistency in correlation among the AR-
114 A scores (Supplementary Fig. S2B-D). Given that Bluemn's AR-A score (14) correlated well with other
115 scores (Supplementary Fig. S2E-G) and the 10 genes in this signature consistently represented AR targets
116 in multiple clinical datasets (Supplementary Fig. S2D; Supplementary Table S2), we decided to use this
117 AR-regulated gene list for our AR-A quantification.
118

119 **Normal prostate epithelium shows a negative correlation between Stemness and AR-A.**
120 The normal human prostate (NHP) comprises 2 major epithelial types: basal and luminal cells
121 (Supplementary Fig. S3A). We annotated two studies that profiled FACS-purified NHP luminal and basal
122 cell populations (19,20) and observed that the luminal cell population (Trop2^{+}CD49f^{lo}) possessed higher
123 *AR* mRNA levels and AR-A but lower Stemness compared to basal cells (Trop2^{+}CD49f^{hi}) and, in both
124 datasets, AR-A negatively correlated with Stemness (Supplementary Fig. S3B-C). These results support
125 that the NHP basal cell compartment harbors primitive stem cells (7,19-22) and AR-A measures the level
126 of prostate epithelial differentiation.
127

128 **Pri-PCa exhibits concordantly increased Stemness and AR-A, and neoadjuvant ADT (nADT)**
129 **decreases both Stemness and AR-A.**
130 In analyzing AR-A and Stemness in matched pairs of prostate tumor (T) and normal (N; tumor-adjacent
131 benign) tissues in the TCGA-PRAD (18; n=51 pairs), Wyatt 2014 (23; n=12 pairs), and Long 2020 (24;

132 n=10 pairs) cohorts, we observed concordantly increased AR-A and Stemness (Fig. 1A-C). Accompanying
133 elevated AR-A, *AR* mRNA levels were also increased in Pri-PCa compared to benign tissue (Fig. 1A-C;
134 note that the increase in *AR* mRNA levels in the Long 2020 cohort approached statistical significance).
135 The paired T/N comparisons (Fig. 1A-C) suggest that early PCa initiation and growth are characterized by
136 concordantly increased Stemness and AR-A. To test whether AR-A might causally drive increased
137 Stemness early during prostate tumorigenesis, we investigated 4 PCa nADT (i.e., ~2-6 months of ADT
138 before prostatectomy or radiation) cohorts (24-26). In the first 3 cohorts with matched pairs of pre- and
139 post-nADT samples (from the same patients), nADT concordantly downregulated AR-A (without
140 decreasing *AR* mRNA levels) as well as the Stemness (Fig. 1D-F). In the Nastiuk cohort with non-paired
141 post-nADT and no-nADT samples (i.e., from different patients but matched for ages and tumor grades and
142 stages), nADT increased *AR* mRNA levels (Supplementary Fig. S4A) but reduced both AR-A and
143 Stemness (Supplementary Fig. S4B-C).
144
145 **Pri-PCa progression is accompanied by reduced AR-A but continually increasing Stemness.**
146 We next assessed the dynamic changes of Stemness and AR-A during *spontaneous* (i.e., therapy-free)
147 Pri-PCa progression (Fig. 2). To this end, we sorted out treatment-naïve tumors in TCGA-PRAD by
148 excluding samples from patients who received adjuvant (post-surgery) hormone therapy (i.e., Pri-PCa/ADT
149 or Tx; n=70) (Fig. 2A) and grouped the Pri-PCa samples according to increasing GS (Fig. 2B-D). When
150 compared with the 52 benign (N) samples, all the four GS groups from Pri-PCa (GS6, GS7, GS8, and
151 GS9/10 combined) showed higher AR-A and Stemness (Fig. 2C-D), consistent with the results in pairwise
152 T/N comparisons (Fig. 1A-C). However, when compared to GS6 PCa, the three higher GS groups showed
153 increasing *AR* mRNA levels (Fig. 2B) but decreasing AR-A (Fig. 2C) and increasing Stemness (Fig. 2D).
154 Jonckheere-Terpstra's (J-T) trend test validated a gradual reduction in canonical (pro-differentiation) AR
155 signaling but an increasing trend of Stemness with Pri-PCa progression (Fig. 2C-D). Notably, although we
156 observed a modest positive correlation between AR-A and Stemness in pooled Pri-PCa samples
157 (Pearson's r=0.27; Fig. 2E), this positive correlation gradually diminished with PCa progression when we
158 categorized the samples by tumor grade (Fig. 2F). The linear regression analysis confirmed that the
159 interaction between Stemness and AR-A significantly depended on tumor grade (P=0.0003), with a linear
160 decrease in the slope of the correlation as GS increased (Fig. 2G).
161 Collectively, these results indicate that, in contrast to early tumorigenesis, *spontaneous PCa*
162 *progression (i.e., with increasing GS and tumor grade) is marked by a divergence between oncogenic*
163 *Stemness and pro-differentiation AR-A*.
164
165 **Therapies and metastatic progression drive further divergence between attenuated AR-A and**
166 **increased Stemness.**

167 Next, we asked how clinical treatment and metastatic progression may impact the Stemness and AR-A by
168 querying untreated Pri-PCa and Pri-PCa/ADT from TCGA and mCRPC in SU2C (10) (Fig. 3A-C). AR-A
169 was elevated in Pri-PCa compared to adjacent benign tissue (N) but reduced in more aggressive Pri-
170 PCa/ADT samples, while the Stemness, in contrast, continually increased from N → Pri-PCa → Pri-
171 PCa/ADT (Fig. 3B-C). Strikingly, mCRPC, despite markedly upregulating *AR* mRNA (Fig. 3A), showed the
172 lowest AR-A but highest Stemness (Fig. 3B-C), *indicating a shift from a positive correlation between AR-*
173 *A and Stemness in Pri-PCa to a negative association in mCRPC* (Fig. 3D).

174 By employing normalized RNAseq data from the PCa transcriptome atlas (Bolis 2021), which
175 included normal prostate specimens (n = 174), Pri-PCa (n = 714) and mCRPC (n = 335) (27), we tracked
176 the Stemness and AR-A across the PCa spectrum (Fig. 3E). AR-A increased from benign to Pri-PCa but
177 declined in Pri-PCa/ADT and continued to decrease in mCRPC, reaching its lowest in mCRPC-NE (28) as
178 supported by J-T test (Fig. 3E). In contrast, the Stemness exhibited a continually increasing trajectory
179 across the PCa spectrum encompassing Normal/Benign → treatment-naïve Pri-PCa → Pri-PCa/ADT →
180 (m)CRPC (P<0.0001, J-T Trend test; Fig. 3F; Supplementary Fig. S5A). Notably, the 3 subtypes of mCRPC,
181 i.e., AR-positive (ARPC), CRPC-NEPC and AR^-/NE^- double-negative PCa (DNPC) all showed higher
182 Stemness than Pri-PCa and also displayed increasing Stemness among the 3 subtypes (Supplementary
183 Fig. S5B). Unexpectedly, tumor-adjacent benign prostate tissues showed much higher Stemness than
184 normal prostate in Genotype-Tissue Expression Project (GTEx; 29) (Fig. 3F; Supplementary Fig. S5A),
185 the majority of which were from cancer-free organ donors. This surprising finding suggests that the
186 transcriptomes of adjacent benign tissues have apparently skewed towards those of cancer samples,
187 consistent with previous observations that adjacent benign tissues represent an intermediate state
188 between healthy and tumor tissues (30). Also of interest, the Cancer Cell Line Encyclopedia (CCLE) (31,32)
189 cell lines including PCa cell lines, and PCa-derived PDX (33) and xenografts (34) exhibited the highest
190 Stemness (Fig. 3F; Supplementary Fig. S5A), supporting that cancer cell lines and xenografts are clonally
191 derived and highly enriched in cancer stem cells.

192 As in our early dissection of the relationship between AR-A and Stemness during spontaneous Pri-
193 PCa progression (Fig. 2F-G), analysis of the Bolis 2021 PCa transcriptome atlas (27) revealed a similar
194 change from a positive correlation between AR-A and Stemness in Pri-PCa (blue line; Pearson's r=0.32,
195 P<0.0001; Fig. 3G) to a negative correlation between the two in mCRPC (green line; Pearson's r=-0.15,
196 P=0.005; Fig. 3G). We further extended our Stemness and AR-A interrogation to include microarray-
197 derived transcriptomic datasets (35,36), allowing us to access data from PCa cohorts generated before
198 the Next-generation sequencing (NGS) era. Analyzing the GRID database of over 82,000 prospectively
199 collected biopsy samples of localized PCa from clinical use of the Veracyte Decipher test (35), we
200 systematically quantified the Stemness across the NCCN Risk Groups and observed increasing Stemness
201 along the NCCN Risk trajectory (Fig. 3H). Likewise, in the Taylor dataset (36), we observed that AR-A was
202 the highest in Pri-PCa but significantly decreased in metastatic PCa (mPCa) (Fig. 3I) while the Stemness

203 increased progressively from benign to Pri-PCa and reached the highest levels in mPCa (Fig. 3J). Linear
204 regression analysis confirmed a gradual loss of positive correlation between AR-A and Stemness during
205 PCa progression, as illustrated by distinct regression lines for each stage (Fig. 3K-M).

206 Finally, we analyzed the dynamic changes of Stemness and AR in genetically engineered mouse
207 models (GEMMs) of PCa with increasing aggressiveness due to individual or combined deletion of 3 tumor
208 suppressor genes, *Pten*, *Rb1* and *Trp53* (37). Briefly, *Pten*$^{-/-}$ single knockout (SKO) prostate tumors
209 develop around 9 weeks, and mice rarely develop metastasis with a median lifespan of 48 weeks. In
210 contrast, the *Pten*$^{-/-}$;*Rb1*$^{-/-}$ double knockout (DKO) mice develop highly metastatic PCa that shortens
211 median survival to ~38 weeks. When *Trp53* is further deleted in DKO background, the triple KO (TKO;
212 *Pten*$^{-/-}$;*Rb1*$^{-/-}$;*Trp53*$^{-/-}$) tumors are exclusively AR^{-} NEPC and castration-resistant *de novo* with high
213 metastatic rate and lifespan of ~16 weeks (37). We found that the AR-A was the highest in SKO tumors
214 but much reduced in aggressive DKO and TKO tumors (Supplementary Fig. S5C). In contrast, Stemness
215 was the lowest in SKO but significantly increased in DKO and TKO (Supplementary Fig. S5D). Correlation
216 analyses revealed a positive correlation between AR-A and Stemness in SKO that turned to negative
217 correlations in both DKO and TKO tumors (Supplementary Fig. S5E-H).

218 The above results, collectively, indicate that *hormone therapy and metastatic progression further*
219 *drive marked increases in Stemness with concomitant decreases in prodifferentiation AR-A*.

220

221 **Stemness is prognostic of poor survival in PCa patients.**

222 We investigated global Stemness and its prognostic significance, and observed that high Stemness
223 consistently correlated with worse patient survival across various cohorts including the Spratt 2017 (38)
224 (P=0.001, log-rank; Fig. 4A), Tosoian 2020 (39) (P=0.014, log-rank; Fig. 4B), CHAARTED 2021 (40)
225 (P=0.006, log-rank; Fig. 4C; P=0.149, log-rank; Supplementary Fig. S6A), and the mCRPC (SU2C 2019
226 (41); P=0.06, log-rank; Supplementary Fig. S6B-C) as well as Taylor 2010 (36) (P=0.028, log-rank;
227 Supplementary Fig. S6D-E). Notably, the CHAARTED cohorts displayed the highest mean Stemness
228 compared to Tosoian and Spratt cohorts, and the CHAARTED cohort showed the highest median Decipher
229 Prostate Genomic Classifier (38-40) among the three cohorts (Fig. 4D). Interestingly, like high Stemness,
230 low AR-A was correlated with poor patient survival in the Taylor dataset (P=0.040, log-rank; Supplementary
231 Fig. S6F).

232

233 **Stemness-high PCa are associated with aggressive molecular subtypes and a 12-gene PCa-Stem**
234 **signature prognosticates poor patient survival.**

235 To identify key drivers of Stemness and explore differences between tumors with high versus low
236 Stemness, we stratified Pri-PCa (TCGA-PRAD) and mCRPC (SU2C 2019) samples separately based on
237 Stemness scores (Fig. 5A). Differential gene expression (DEG) analyses revealed significant differences
238 between the top 33% (Stemness-high) and the bottom 33% (Stemness-low) PCa samples in both

239 treatment-naïve Pri-PCa (Fig. 5B) and treatment-failed mCRPC (Fig. 5C), resulting in a 12-gene '**PCa-**
240 **Stem signature**' (Fig. 5D; Supplementary Table S2).

241 Gene set enrichment analysis (GSEA) was performed to delineate the molecular differences between
242 Stemness-low and Stemness-high PCa samples (Fig. 5E-F). GSEA revealed that Stemness-high PCa
243 samples were enriched in gene sets associated with embryonic stem cells (ESC), as well as aggressive
244 cancer phenotypes, such as undifferentiated cancer and metastasis, in both Pri-PCa and mCRPC (Fig.
245 5F). In contrast, Stemness-low PCa samples were enriched in gene signatures linked to lower
246 aggressiveness and inflammatory pathways (Fig. 5E). Additionally, hallmark pathways such as E2F targets,
247 MYC targets, mTORC1 signaling, and DNA repair were upregulated in Stemness-high PCa (Fig. 5F), while
248 TGF-β signaling, TNF-α signaling, and IFN-γ responses were prominent in Stemness-low PCa (Fig. 5E).

249 The aggressive PAM50-LumB molecular subtype (42-44) was significantly more prevalent in
250 Stemness-high PCa, accounting for 74% in Pri-PCa (compared to 15% in Stemness-low PCa; Fig. 5G)
251 and 43% in mCRPC (compared to 4% in Stemness-low PCa; Fig. 5H). The PCS1 subtype (45,46), known
252 for its association with ADT resistance and the highest risk of progression to advanced disease in
253 comparison with PCS2 or PCS3, was predominantly enriched in both Stemness-high Pri-PCa and mCRPC
254 (Fig. 5I-L). Notably, the PAM50-Basal subtype (42,43) increased in Stemness-high mCRPC but not in Pri-
255 PCa (Fig. 5G-H), aligning with the characteristics of mCRPC, which involves lineage plasticity and
256 acquisition of basal, mesenchymal, neural and stem-like phenotypes when developing ARPI
257 resistance (7,44,47). Consequently, Stemness-high samples remained largely AR-dependent (48) in Pri-
258 PCa (Fig. 5M) but transitioned to AR-independent NE subtype (44) in mCRPC (Fig. 5N). Stemness-high
259 PCa was also characterized by high proliferation as evidenced by their enrichment in a 31-gene cell-cycle
260 progression signature (44) (Fig. 5O-P). Finally, we examined the association between Stemness and a
261 signature of lineage plasticity risk after Enza treatment for mCRPC (12) and found that Stemness-high
262 tumors may be at risk for this virulent form of treatment resistance (Fig. 5Q-R).

263 To further assess the clinical relevance of Stemness, we analyzed the prognostic impact of our newly
264 developed 12-gene PCa-Stem signature (Fig. 5D). We observed that higher PCa-Stem signature
265 correlated with worse patient survival in both Pri-PCa (P<0.0001, log-rank; Fig. 5S-T) and mCRPC
266 (P<0.0001, log-rank; Fig. 5U-V) patients. Multivariate analysis, adjusted for clinicopathologic parameters
267 such as age, GS and stage, showed that patients with high PCa-Stem signature had significantly worse
268 independent prognosis compared to those with low PCa-Stem signature. This was demonstrated by worse
269 progression-free survival (PFS) in Pri-PCa (multivariable-adjusted HR=1.636 (1.014 – 2.64), P=0.0438;
270 Fig. 5T) and overall survival (OS) in mCRPC (multivariable-adjusted HR=4.712 (2.011 – 11.04), P<0.001;
271 Fig. 5V), respectively. Furthermore, the PCa-Stem signature steadily and continually increased across the
272 PCa evolutionary spectrum and correlated with PCa disease progression scores as supported by trajectory
273 inference analysis of the Bolis (27) PCa transcriptome atlas (Pearson's r=0.72; Supplementary Fig. S7A-
274 B). Strikingly, gene expression analysis revealed that 11 of the 12 genes (except *KLK12*) in the PCa-Stem

275 signature significantly correlated with the PCa disease progression (Supplementary Fig. S7C). In contrast,
276 among the genes commonly downregulated in Stemness-high PCa samples in both Pri-PCa and mCRPC
277 (Supplementary Table S3), some (e.g., *PTGDS*, *SPARCL1*, *CLU*, *GJA1* and *S100A4*) were involved in
278 regulating prostate-specific glandular structures and luminal functions while others (e.g., *FBLN1*, *SFRP1*,
279 *IGFBP6*, *GAS1* and *TIMP2*) played general roles in epithelial differentiation (Supplementary Fig. S7D).
280 Overall, these findings indicate that *PCa with high Stemness exhibit greater aggressiveness, a higher*
281 *likelihood of developing lineage plasticity and therapy resistance, and poor survival outcomes*.
282
283 **Stemness-high PCa have high tumor mutation burden (TMB) and unique genomic features.**
284 We determined the potential differences in genomic features between Stemness-high vs. Stemness-low
285 PCa and found that mCRPC had a higher fraction of altered genome (Fig. 6A) and higher TMB (Fig. 6B)
286 than Pri-PCa. In both Pri-PCa and mCRPC, Stemness-high PCa displayed a higher fraction of altered
287 genome (Fig. 6A) and TMB (Fig. 6B) than Stemness-low PCa although there was no difference in patient
288 ages (Fig. 6C). In Pri-PCa, Stemness-high samples had a higher prevalence of *PTEN* deletion (DEL),
289 *SPOP* and *FOXA1* mutations (MUT) and *MYC* amplification (AMP) whereas in mCRPC, Stemness-high
290 PCa had more prevalent *RB1* DEL and *AR* MUT (Fig. 6D-F).
291 Globally, both Pri-PCa and mCRPC exhibited mutations in more than a dozen genes although most
292 of these alterations were <10% (Supplementary Fig. S8A; green symbols), consistent with reports that
293 PCa is genomically heterogeneous with a broad spectrum of genomic alternations of low penetrance
294 (49,50). On the other hand, homozygous deletion (HOMDEL) events, particularly, loss of *PTEN* and *RB1*,
295 occurred frequently in both Pri-PCa and mCRPC (Supplementary Fig. S8A; blue symbols) whereas AMP
296 events in oncogenes such as *MYC* were more prevalent in mCRPC (Supplementary Fig. S8A; red
297 symbols). Nevertheless, *PTEN* and *RB1* DEL represented among the most prevalent alterations in early-
298 stage (GS6) PCa (Supplementary Fig. S8B-C). Analysis of genetic alterations across the spectrum of PCa
299 progression revealed that among the 3 tumor suppressors (*RB1, PTEN* and *TP53*), while homozygous
300 *RB1* DEL remained relatively constant at 13%, 6%, 10% and 10% in low-grade (GS6), high-grade (GS9/10),
301 treated Pri-PCa and mCRPC, respectively, *PTEN* HOMDEL (9%, 23%, 30% and 26%) and *TP53* MUT
302 (0%, 21%, 27% and 37%) continued to increase along this progression (Supplementary Fig. S8B-C).
303 Among the 3 oncogenic events analyzed, while high levels of *TMPRSS2* fusions (~40%) remained
304 unchanged from low-grade to high-grade Pri-PCa to mCRPC, *MYC* (2%, 12%, 19% and 24%) and *AR* (0%,
305 1%, 6% and 49%) AMP continued to increase along the progression trajectory (Supplementary Fig. S8B-
306 C). In fact, prevalent *AR* MUT (11%) were observed only in the most aggressive and Stemness-highest
307 mCRPC (Supplementary Fig. S8B-C), suggesting potentially high noncanonical AR-A in mCRPC.
308 Analyzing these major genomic alterations in association with PCa Stemness, we observed that *RB1* DEL,
309 *FOXA1* (together with *SPOP*, *IDH1*, and *CHD1*) MUT, and especially *MYC* AMP were significantly

310 associated with increased Stemness in Pri-PCa (Supplementary Fig. S8D). In mCRPC, only *RB1* DEL
311 exhibited a statistically significant association with higher Stemness (Supplementary Fig. S8E).
312
313 **MYC further drives Stemness during spontaneous PCa progression.**
314 *AR* AMP and MUT are exclusively treatment-induced as there were virtually no *AR* genomic alterations in
315 treatment-naïve Pri-PCa (Supplementary Fig. S8B-C). We showed that early during PCa development
316 increased AR-A may drive elevated Stemness (Fig. 1D-F); however, treatment-naïve Pri-PCa displayed
317 continually increasing Stemness but decreasing AR-A (Fig. 2). What could be driving persistently high
318 Stemness during Pri-PCa progression with decreasing AR-A and in the absence of *AR* genomic alterations?
319 We found that Stemness-high Pri-PCa, compared to Stemness-low Pri-PCa, were enriched in MSigDB
320 Hallmark MYC_TARGETS (MYC_Targets_V1 and MYC_Targets_V2; Fig. 5F) and had more prevalent
321 *MYC* AMP (Fig. 6D and 6F). High-grade (GS9/10) Pri-PCa also had more *MYC* AMP events than low-
322 grade (GS6) Pri-PCa (12% vs. 2%; P=0.006, χ^2 test; Supplementary Fig. S8C). Importantly, *MYC* AMP
323 was most prominently associated with increased Stemness in Pri-PCa (Supplementary Fig. S8D). These
324 observations led us to hypothesize that MYC may represent a critical Stemness driver during spontaneous
325 Pri-PCa progression (in absence of therapeutic pressure). To test this hypothesis, we quantified MYC
326 signaling activity (MYC-sig; See Methods and Supplementary Table S2 for gene signature information)
327 (51) across the PCa progression spectrum. We observed that: 1) both *MYC* mRNA and MYC-sig increased
328 in Pri-PCa compared to matched benign samples (Fig. 7A-B); 2) MYC-sig continued to go up during Pri-
329 PCa progression (Fig. 7C); 3) unlike nADT-induced concomitant decline in both AR-A and Stemness (Fig.
330 1D-F; Supplementary Fig. S4), nADT showed no discernible effect on MYC-sig (Supplementary Fig. S9A-
331 D); and 4) MYC-sig continued to increase across the disease spectrum with mCRPC exhibiting the highest
332 MYC activity (Fig. 7D-E) and with MYC-sig positively correlated with the Stemness (Fig. 7F-H).
333 *These results, together, support MYC as a Stemness driver during PCa progression*.

DISCUSSION

The current project was undertaken to quantitatively co-analyze the global changes of and the interrelationship between cancer stemness and pro-differentiation AR signaling activity during PCa evolution. By employing gene expression-based general Stemness and AR-A signature scores and through developing a new 12-gene PCa-Stem signature, we show that while the differentiation-regulating AR-A steadily declines in the PCa continuum, pervasively increasing Stemness quantitatively measures PCa aggressiveness, plasticity and progression, and represents a poor prognosticator for patient outcomes. We report that Stemness-high PCa possess unique genomic features with high TMBs and are associated with aggressive molecular subtypes. We further present evidence that elevated Stemness in early PCa might be driven by increased AR-A but increased MYC-sig activity and other genomic alterations likely propagate the exponentially increased Stemness in mCRPC where AR-A is suppressed.

Early studies reported that a cohort of AR-regulated genes declines in high-grade versus low-grade Pri-PCa (52,53) and that loss of AR expression or inhibition of AR-A promotes a stem-like phenotype (8,34,54,55). However, the global pro-differentiation AR-A and cancer stemness have not been systematically and quantitatively assessed and co-analyzed in PCa, and it's unclear whether PCa progression is accompanied by increased stemness as in some other cancers such as glioblastoma and breast cancer (6). Our analysis demonstrates that PCa progression is accompanied by a continual increase in Stemness (score) but loss of canonical AR-A, with the two inversely correlated with each other (Supplementary Fig. S10). Importantly, the Stemness tracks treatment-induced plasticity and PCa aggressiveness, and both high global Stemness and high PCa-Stem signature prognosticate poor patient survival. To our knowledge, this is the first comprehensive study to simultaneously quantify the oncogenic stemness and pro-differentiation AR-A across the PCa continuum.

The normal prostatic acini and ducts are lined by AR^+ secretory luminal cells and AR^- basal cells together with rare neuroendocrine cells. We find that the NHP luminal cells have higher AR-A compared to basal cells, confirming AR-A as a metric for quantifying canonical AR activity and prostatic epithelial differentiation. On the other hand, basal cells have higher Stemness, consistent with earlier findings from our lab (19) and others (20-22,56) showing the basal cell compartment harbors stem cells. Oncogenic transformation is known to confer stem-like features in the initiated cells. Indeed, compared to adjacent benign tissue, Pri-PCa exhibit elevated Stemness, which is associated with and likely driven by increased AR-A. Loss of *PTEN* and *RB1* (9% and 13%, respectively, in GS6 tumors) could also potentially contribute to increased Stemness in early prostate tumors. Interestingly, tumor-adjacent benign tissues display higher Stemness than normal prostate, suggesting that these benign tissues are not normal.

368 In treatment-naïve Pri-PCa, tumor progression is accompanied by decreasing AR-A but persistently
369 high Stemness (Supplementary Fig. S10). The decreasing AR-A is driven by progression-related loss of
370 differentiation while increasing Stemness is likely driven by *MYC* amplification and increased MYC activity
371 with contributions from other oncogenic evens such as loss of *PTEN* and *RB1*. Long-term ADT/ARPI
372 treatment, as expected, further attenuates AR-A but substantially upregulates the Stemness such that
373 mCRPC have the highest Stemness, which is probably driven by continually increasing genomic alterations
374 such as *MYC* amplification and loss of tumor suppressors. Notably, as *AR* alterations (AMP/MUT) are
375 exclusively induced by ARPIs, noncanonical AR-A (i.e., castration-resistant AR activity) likely make
376 significant contributions to the increased Stemness in mCRPC.
377
378 What biological correlates does our Stemness metric measure? *First*, it measures transcriptional
379 features and relative abundance of stem cells and CSCs. Therefore, the NHP basal/stem cells display
380 higher Stemness than luminal cells (consistent with literature (19-22)); ARPI treatment, while shutting down
381 AR signaling, enriches CSCs (7,34,54,55) and upregulates Stemness (this study); and PCa cell lines,
382 xenografts and PDX, known to be clonally derived from cancer stem/progenitor cells, demonstrate the
383 highest Stemness. *Second*, it measures cellular and lineage plasticity induced by treatment and genetic
384 alterations. Thus, mCRPC, which harbor more abundant treatment-reprogrammed $AR^{-/lo}$ cells and PCa
385 cells with stem-like features or in an AR-indifferent state (8,12-14,16,33,47,48), manifests the highest
386 Stemness. Our analysis further substantiates the aggressive nature of ($AR^{-/lo}$) CRPC-NEPC and DNPC
387 compared to ARPC, as evidenced by their elevated PCa-Stem signature scores. This suggests a shift in
388 the phenotypic landscape of mCRPC towards more stem-like and aggressive forms, particularly under the
389 pressure of advanced therapies. Likewise, aggressive DKO and TKO murine prostate tumors have
390 undergone lineage transformation and also exhibit higher Stemness than indolent SKO tumors. *Third*, the
391 Stemness metric likely reports the high proliferative status of advanced PCa and mCRPC, as Stemness-
392 high tumors in both Pri-PCa and mCRPC are enriched in "Cell-cycle progression" signature and most
393 genes in the 12-gene PCa-Stem Signature are involved in mitosis and cell-cycle progression. *Finally*, the
394 Stemness score measures PCa aggressiveness as high Stemness correlates not only with more advanced
395 and aggressive stages of PCa but also with aggressive PAM50-LumB and PCS1 molecular subtypes.
396
397 Of clinical significance, both the 12-gene PCa-Stem signature and the global Stemness score
398 correlate with poor patient survival, suggesting the possibility of developing the Stemness metric into a
399 predictive biomarker to distinguish aggressive from indolent primary tumors and a prognostic indicator of
400 unfavorable clinical outcomes in mCRPC patients. Notably, 11 of the 12 genes (except *KLK12*) in the newly
401 developed PCa-Stem signature are significantly correlated with PCa progression (Supplementary Fig. S7C)
402 implicating their individual contributions to the increased Stemness in advanced Pri-PCa and mCRPC.
403 Analysis using data from The Human Protein Atlas (www.proteinatlas.org) reveals that these 11 genes are

also recognized as unfavorable prognostic markers in PCa and several other cancers (Liu X and Tang, unpublished), raising the potential utility of the PCa-Stem signature as a prognostic marker not only for PCa but also for other malignancies. Coupled with earlier studies linking increased Stemness with aggressive breast and brain cancer subtypes (6), our findings herein underscore the increased Stemness as a 'universal' and fundamental characteristic of cancer progression and aggressiveness.

We recognize that the Stemness algorithm utilized in our studies was not developed specifically for PCa and therefore, its sensitivity to distinguish subtle intra-group differences remains to be fully validated. The bulk RNA-seq data used to derive Stemness and AR-A was not from pure epithelial cancer cells, a technical issue that can be potentially amended by scRNA-seq analysis and other Stemness pipelines such as the CytoTRACE (57,58) and by using cancer-sepcific genomic features derived, for example, from cell-free DNA (59). Finally, it will be important to determine whether and how noncanonical (castration-associated) AR signaling (driven by *AR* AMP/MUT) may contribute to the highest Stemness in mCRPC.

In conclusion, we have developed transcriptome-based gene signature scores to assess pro-differentiation AR activity (AR-A), MYC activity (MYC-sig) and oncogenic stem-cell features (general Stemness score and the 12-gene PCa-Stem signature). These scores enable us to globally profile differentiation and aggressiveness status across the PCa progression spectrum. This work advances our understanding of dynamic evolution of AR-A and cancer stemness during PCa progression and therapy resistance, and the signature scores reported herein have the potential to serve as clinical classifiers and aid in the identification of patients who may benefit from stemness-targeting therapies.

METHODS

PCa clinical datasets and data collection

In this study, we utilized a total of 26 published and in-house prostate cancer (PCa) related datasets, including various cohorts encompassing the evolutionary spectrum of PCa (Supplementary Fig. S1A-B): normal prostate, tumor-adjacent benign tissue, treatment-naïve primary PCa (Pri-PCa) with increasing GS, PCa treated with neo-adjuvant ADT (nADT) or long-term ADT, metastatic castration-resistant PCa (mCRPC), and PCa cell lines, PCa patient-derived xenografts (PDX) and xenografts. Clinical information, genomic data and gene expression profiling data were downloaded and detailed information on each dataset is listed in Supplementary Table S1. Dataset descriptions include dataset source references, PubMed IDs (PMIDs; RRID:SCR_004846), DOI links, sample type and source (e.g., normal prostate tissue, adjacent benign prostate tissue or primary culture from PCa patient, primary or metastatic prostate tumor, xenografts, cell lines), sample sizes, data types used in the current study (clinicopathologic data, RNAseq, microarray, whole exome sequencing [WES]), and public data access portals.

Data Access and Repository Information:

Data for this study were retrieved from the following public repositories and databases, with persistent identifiers where applicable:

1. GTEx Portal (RRID:SCR_013042; https://gtexportal.org/)
2. Gene Expression Omnibus (GEO; RRID:SCR_005012; https://www.ncbi.nlm.nih.gov/geo/)
3. cBioPortal for Cancer Genomics (RRID:SCR_014555; https://www.cbioportal.org/)
4. Zenodo Repository (RRID:SCR_004129; https://zenodo.org/)
5. Decipher GRID Database (RRID:SCR_006552; ClinicalTrials.gov identifier: NCT02609269)
6. European Genome-phenome Archive (EGA; RRID:SCR_004944; https://ega-archive.org/)
7. European Nucleotide Archive (ENA; RRID:SCR_006515; https://www.ebi.ac.uk/ena/browser/home)
8. UCSC Xena Functional Genomics Portal (RRID:SCR_018938; https://xenabrowser.net/)

Detailed dataset accession numbers and portal links for each dataset are provided in Supplementary Table S1.

The 26 datasets are briefly described below:

1) **GTEx 2013** (PMID: 23715323)(29): The Genotype-Tissue Expression (GTEx) Project repository collected high-throughput and clinical data of normal tissue from many organs. RNAseq data of 245 normal prostate tissue samples was downloaded from the GTEx portal (RRID:SCR_013042; ref. 29; DOI: 10.1038/ng.2653; https://www.gtexportal.org/, version: v8).

2) **Smith 2015** (PMID: 26460041)(20): RNAseq data of 5 prostate basal cell samples (Trop2^{+}CD49f^{hi}) and corresponding 5 luminal cell samples (Trop2^{+}CD49f^{lo}) FACS-purified from benign human prostate

tissue in 5 PCa patients (n=5) was retrieved from the GEO database GSE82071 (ref. 20; DOI: 10.1073/pnas.1518007112).

3) **Liu 2016** (PMID: 27926864)(56): RNAseq data of 3 FACS-purified human prostate basal cell samples ($CD45^{-}EpCAM^{+}CD49f^{hi}CD38^{lo}$) with corresponding luminal ($CD45^{-}EpCAM^{+}CD49f^{lo}CD38^{hi}$) and luminal progenitor ($CD45^{-}EpCAM^{+}CD49f^{lo}CD38^{lo}$) cell populations purified from the benign prostate tissues of 3 PCa patients (n=3) was retrieved from the supplementary data from Liu et al., 2016 (56). The microarray-based transcriptomic profiles of the same samples were retrieved from the GEO database GSE89050 (ref. 56; DOI: 10.1016/j.celrep.2016.11.010).

4) **Zhang 2016** (PMID: 26924072)(19): RNAseq data of 3 human prostate basal cell ($Trop2^{+}CD49f^{hi}$) with the corresponding 3 luminal cell ($Trop2^{+}CD49f^{lo}$) samples FACS-purified from benign prostate tissues of 3 PCa patients (n=3) was retrieved from the GEO database GSE67070 (ref. 19; DOI: 10.1038/ncomms10798).

5) **TCGA PRAD 2015** and **Pan-Cancer Atlas 2018**: The Cancer Genome Atlas (TCGA) (https://www.cancer.gov/tcga) repository collected high-throughput molecular and clinical data from primary cancer and matched normal/benign samples spanning 33 human cancer types, including prostate adenocarcinoma (PRAD). For each cancer type, TCGA published an initial "marker papers" summarizing analyses performed. Supplemental and associated data files supporting these "marker papers" are available through the NCI Genomic Data Commons (GDC) website (https://gdc.cancer.gov/about-data/publications). For prostate cancer, **TCGA PRAD 2015** (PMID: 26544944; ref. 18; DOI: 10.1016/j.cell.2015.10.025) is the marker paper on PCa published in 2015, which includes the dataset of 333 primary prostate adenocarcinomas (281 treatment-naïve Pri-PCa, 49 PCa with post-surgery adjuvant ADT, and 52 matched normal/benign prostate tissue). Genomic data were obtained from **cBioPortal for Cancer Genomics** (RRID:SCR_014555; https://www.cbioportal.org), specifically the TCGA-PRAD Firehose Legacy study (https://www.cbioportal.org/study/summary?id=prad_tcga). RNAseq expression data was obtained from Zhang et al., 2020 (PMID: 32350277; ref. 16; DOI: 10.1038/s41467-020-15815-7).

Further clinical and molecular annotations for prostate cancer were expanded in the TCGA Pan-Cancer Atlas project (**TCGA PRAD 2018 (Pan-Cancer Atlas)**), covering 494 patients with Pri-PCa (422 treatment-naïve Pri-PCa, 70 PCa with post-surgery adjuvant hormone treatment, 2 PCa with chemotherapy, and 52 matched adjacent normal/benign prostate tissue). Clinicopathologic features (age, Gleason scores, PSA levels, tumor stages) and genomic alterations (mutations, copy number variations [CNVs], structural variants [SVs]) were retrieved from **cBioPortal Pan-Cancer Atlas** (https://www.cbioportal.org/study/summary?id=prad_tcga_pan_can_atlas_2018) and from the Pan-Cancer Atlas companion site (https://www.cell.com/pb-assets/consortium/pancanceratlas/pancani3/index.html). Survival data were obtained from Liu et al., 2018 (PMID: 29625055; DOI: 10.1016/j.cell.2018.02.052)(60). Normalized RNAseq data were

496 downloaded via NCI GDC hub at UCSC Xena Functional Genomics Portal (https://gdc.xenahubs.net,
497 version 2019-07-20; DOI: 10.1038/s41587-020-0546-8).
498 6) **Rajan 2014** (PMID: 24054872)(25): Clinicopathologic (Gleason scores) and RNAseq data of 7 matched
499 pre- and post-nADT PCa samples were obtained, respectively, from Table 1 in Rajan et al., 2014 (ref.
500 25; DOI: 10.1016/j.eururo.2013.08.011) and the GEO database GSE48403.
501 7) **Sharma 2018** (PMID: 30314329)(26): Clinicopathologic (Gleason scores) and RNAseq data of 7
502 matched pre- and post-nADT PCa samples from the responder group (also defined as "Low Impact
503 Group" in the source reference) was obtained, respectively, from supplementary Table 1 in Sharma et
504 al., 2018 (ref. 26; DOI: 10.3390/cancers10100379) and the GEO database GSE111177.
505 8) **Long 2020** (PMID: 32951005; DOI: 10.1016/j.eururo.2013.08.011)(24): RNAseq data of 6 matched pre-
506 and post-nADT PCa samples was obtained from the GEO database GSE82071. Additionally, RNAseq
507 data from 10 locally advanced PCa samples along with their paired adjacent benign prostate tissues
508 were obtained from the GEO database GSE82071.
509 9) **Nastiuk (RPCI) 2020** (submitted; ref.(61)): Clinicopathologic data (Gleason scores) and RNAseq data
510 of 43 Pri-PCa samples from post-nADT PCa patients and 43 tumor samples from age-, stage-,
511 clinically-matched PCa patients without nADT was obtained from Jamroze et al., 2024 (work led by
512 Drs. K. Nastiuk and G. Chatta at the Roswell Park Comprehensive Cancer Center). RNAseq data and
513 clinicopathologic information from the Nastiuk 2020 cohort (unpublished) were provided in-house by
514 Dr. K. Nastiuk and are available from the corresponding author upon reasonable request.
515 10) **Gerhauser 2018** (PMID: 30537516; DOI: 10.1016/j.ccell.2018.10.016)(62): RNAseq data of 118
516 primary tumor samples and 9 adjacent benign prostate tissue from early-onset PCa patients was
517 obtained from the European Genome-Phenome Archive (EGA) (https://ega-archive.org), accession
518 number EGAS00001002923.
519 11) **Wyatt 2014** (PMID: 25155515; DOI: 10.1186/s13059-014-0426-y)(23): Clinicopathologic (Gleason
520 scores) and RNAseq data of 12 primary PCa samples from treatment-naïve PCa patients and 12
521 adjacent benign prostate tissue were obtained from the European Nucleotide Archive (ENA)
522 (https://www.ebi.ac.uk/ena/browser/home), accession number PRJEB6530.
523 12) **Spratt 2017** (PMID: 28358655; DOI: 10.1200/JCO.2016.70.2811)(38): Transcriptomic profiles
524 (Microarray) and clinicopathologic data of 855 radical prostatectomy specimens from a multi-
525 institutional study of intermediate- and high-risk localized PCa patients were obtained from Veracyte
526 GRID (https://decipherbio.com/grid/).
527 13) **Tosoian 2020** (PMID: 32231245; DOI: 10.1038/s41391-020-0226-2)(39): Transcriptomic profiles
528 (Microarray) and clinicopathologic data of 405 radical prostatectomy and biopsy specimens from high-
529 risk localized PCa patients were obtained from Veracyte GRID (https://decipherbio.com/grid/).
530 14) **CHAARTED correlatives 2021** (PMID: 34129855; DOI: 10.1016/j.annonc.2021.06.003)(40):
531 Transcriptomic profiles (Microarray) and clinicopathologic data of 160 biopsy specimens from a Phase

3 trial of metastatic hormone-sensitive PCa patients were obtained from the NCTN Data Archive (https://nctn-data-archive.nci.nih.gov), accession number **NCT00309985-D14**.

15) **Decipher GRID Biopsy** (PMID: 37060201; DOI: 10.1002/cncr.34790)(35): Transcriptomic profiles from 82,470 prospectively collected prostate biopsy samples were retrieved from the Decipher GRID database (RRID: SCR_006552; https://decipherbio.com/grid; ClinicalTrials.gov identifier: **NCT02609269;** https://clinicaltrials.gov/ct2/show/NCT02609269). Patient data were de-identified from clinical use of the Decipher prostate genomic classifier in accordance with the Safe Harbor method described in the HIPAA Privacy Rule 45 CFR 164.514(b) and (c) (Veracyte, San Diego, CA). The samples, comprising a large cohort of localized prostate cancer (PCa), were utilized to compare the distribution of Stemness Index values across National Comprehensive Cancer Network (NCCN) risk groups.

<u>Clinicopathologic Breakdown and Risk Group Analysis:</u>

Detailed clinicopathologic review revealed that the majority of the cohort presents with low-grade localized PCa. The TNM staging breakdown includes:

- **T1 stage:** Approximately 50% of samples, indicating early-stage cancer localized within the prostate.
- **T2 stage:** Approximately 8%, representing cancer confined within the prostate but more extensive than T1.
- **T3 and T4 stages:** Less than 1%, suggesting advanced local spread.
- **N0:** Approximately 98%, indicating no regional lymph node involvement.
- **N1:** Approximately 2%, suggesting regional lymph node involvement.

The Decipher GRID database (RRID:SCR_006552) categorizes patients into NCCN risk groups based on TNM stage, PSA level, and Gleason score:

- **Very Low and Low Risk:** T1–T2a, N0, M0, PSA <10 ng/mL, and Gleason score ≤6; often managed with active surveillance or less aggressive treatment.
- **Intermediate Risk – Favorable:** Typically T2b–T2c, N0, M0, PSA 10–20 ng/mL, and Gleason score 7; managed with less aggressive treatment but closer monitoring.
- **Intermediate Risk – Unfavorable:** Similar clinical features to favorable but with higher disease burden or adverse factors requiring careful monitoring.
- **High Risk:** Usually involves T3a, N0, M0, PSA >20 ng/mL, or Gleason score 8–10; often managed aggressively with surgery, radiation, and/or hormonal therapy.
- **Very High Risk:** Typically includes T3b–T4, any N, M0, and high Gleason scores or PSA levels (PSA >20 ng/mL); patients are at significant risk for metastatic progression and are treated aggressively, often with multimodal therapies.

567 Observations on Disease Severity and Treatment Naïvety:
568 Analysis of the cohort indicates that only approximately 13% of cases fall into the High and Very High
569 risk categories (8,376 + 2,399 = 10,775 samples), suggesting that the majority (approximately 87%)
570 are below Intermediate Risk (≤GS7). This distribution implies that most patients were treatment-naïve
571 and likely androgen deprivation therapy (ADT)-free due to less aggressive disease status.
572 16) **Bolis 2021** (PMID: 34857732; DOI: 10.1038/s41467-021-26840-5)(27): RNAseq and clinicopathologic
573 data of 1,223 clinical samples from an integrated cohort consisting of normal prostate specimens
574 (n = 174), Pri-PCa (n = 714) and mCRPC (n = 335) was obtained from the Zenodo repository (Record
575 ID: 5546618; https://zenodo.org/records/5546618). This resource of Prostate Cancer Transcriptome
576 Atlas (https://prostatecanceratlas.org) was built and integrated from the following studies/datasets: (1)
577 Genotype-Tissue Expression Database (GTEx; PMID: 23715323; ref. 29); (2) The Cancer Genome
578 Atlas (TCGA, TCGA-PRAD; PMID: 26544944; ref. 18); (3) Atlas of RNA-sequencing profiles of normal
579 human tissues (GSE120795; PMID: 31015567; ref. 63); (4) Integrative epigenetic taxonomy of PNPCa
580 (GSE120741; PMID: 30464211; ref. 64); (5) Prognostic markers in locally advanced lymph node-
581 negative prostate cancer (PRJNA477449); (6) The long noncoding RNA landscape of NEPC and its
582 clinical implications (PRJEB21092; PMID: 29757368; ref. 65); (7) Integrative clinical sequencing
583 analysis of metastatic CRPC reveals a high frequency of clinical actionability (PRJNA283922; dbGaP:
584 phs000915; PMID: 26000489; ref. 10); (8) CSER—exploring precision cancer medicine for sarcoma
585 and rare cancers (PRJNA223419; dbGaP: phs000673; PMID: 28783718; ref. 66); (9) Molecular basis
586 of NEPC (Beltran 2016; PRJNA282856; dbGaP: phs000909; PMID: 26855148; ref. 28); (10)
587 Heterogeneity of androgen receptor splice variant-7 (AR-V7) protein expression and response to
588 therapy in CRPC (GSE118435; PMID: 30334814; ref. 67); (11) RNAseq of human PCa cell lines and
589 mCRPC tumor (GSE14750; PMIDs: 32460015; ref. 68; 33658518; ref. 69; 34244513; ref. 70 |
590 GSE171729; PMID: 34244513; ref. 70); and (12) Molecular profiling stratifies diverse phenotypes of
591 treatment-refractory metastatic CRPC (PRJNA520923; GEO: GSE126078; PMID: 31361600; ref. 33).
592 17) **Taylor 2010** (PMID: 20579941; DOI: 10.1016/j.ccr.2010.05.026)(36): Transcriptomic profiles
593 (Microarray) and clinicopathologic (recurrence-free survival) data of 29 adjacent benign prostate tissue,
594 131 Pri-PCa, and 19 mPCa were obtained from the GEO database (GSE21034) and the cBioPortal for
595 Cancer Genomics (https://www.cbioportal.org/study/summary?id=prad_mskcc).
596 18) **SU2C 2015** (PMID: 26000489; DOI: 10.1016/j.cell.2015.05.001)(10): Clinical and genomic data of 150
597 mCRPC samples were obtained from the cBioPortal for Cancer Genomics
598 (https://www.cbioportal.org/study/summary?id=prad_su2c_2015). RNAseq data of 98 mCRPC
599 samples was retrieved from Zhang et al., 2020 (PMID: 32350277; ref. 16; DOI: 10.1038/s41467-020-
600 15815-7).
601 19) **SU2C 2019** (PMID: 31061129; DOI: 10.1073/pnas.1902651116)(41): Clinicopathologic data (age,
602 Gleason scores, PSA levels, overall survival) and genomic data of 444 mCRPC samples, and RNAseq

data of 266 mCRPC samples (prepared using poly(A) enrichment for RNAseq library construction), were obtained from the cBioPortal for Cancer Genomics (https://www.cbioportal.org/study/summary?id=prad_su2c_2019).

20) **Labrecque 2019** (PMID: 31361600; DOI: 10.1172/JCI128212)(33): RNAseq data of 98 mCRPC samples and 39 PDX-LuCaP was obtained from the GEO database GSE126078.

21) **Alumkal 2020** (PMID: 32424106; DOI: 10.1073/pnas.1922207117)(13): RNAseq data of 25 mCRPC samples before treatment with enzalutamide (ENZA) was obtained from Supplementary dataset S01 of Alumkal *et al.*, 2020 (ref. 13).

22) **Westbrook 2022** (PMID: 36109521; DOI: 10.1038/s41467-022-32701-6)(12): RNAseq data of 42 mCRPC samples consisting of 21 matched pre/post Enzalutamide treatment samples was retrieved from Westbrook *et al.*, 2022 (ref. 12).

23) **Beltran 2016** (PMID: 26855148; DOI: 10.1038/nm.4045)(28): RNAseq data of mCRPC samples, including 34 castration-resistant adenocarcinoma (mCRPC-Adeno) and 15 neuroendocrine histologies (mCRPC-NEPC) samples, was obtained from cBioPortal for the Cancer Genomics (https://www.cbioportal.org/study/summary?id=nepc_wcm_2016).

24) **Goodrich 2017** (PMID: 28059767; DOI: 10.1126/science.aah4199)(37): RNAseq data of murine prostate tumors from genetically engineering mouse models (GEMMs) of PCa of different genotypes, including 4 SKO (single knockout: PBCre4:*Pten*$^{f/f}$), 13 DKO (double knockout PBCre4:*Pten*$^{f/f}$:*Rb1*$^{f/f}$), and 6 TKO (PBCre4:*Pten*$^{f/f}$:*Rb1*$^{f/f}$:*Trp53*$^{f/f}$) was obtained from the GEO database GSE90891 (*f* = a floxed allele of the indicated genes).

25) **CCLE 2018** (PMID: 22460905; DOI: 10.1038/nature11003)(31): RNAseq data of 1,019 human cell lines were obtained from the Xena Functional Genomics Portal (https://xenabrowser.net, version: 2018-05-30; ref. 71). Among them, eight prostate cancer cell lines — DU145 (RRID:CVCL_0105), LNCaP clone FGC (RRID:CVCL_1379), MDA PCa 2b (RRID:CVCL_4745), NCI-H660 (RRID:CVCL_0459), PC-3 (RRID:CVCL_0035), VCaP (RRID:CVCL_2235), 22Rv1 (RRID:CVCL_1045), and PRECLH (PrEC LH; RRID:CVCL_V626) — were included for analysis.

26) **XG-LNCaP** and **XG-LAPC9** (PMID: 30190514; DOI: 10.1038/s41467-018-06067-7)(34): RNAseq data of 12 LNCaP xenografts (XG-LNCaP) and 10 LAPC9 xenografts (XG-LAPC9) was obtained from the GEO database GSE88752.

Sex as a biological variable

All clinical datasets analyzed in this study consisted exclusively of male patients, consistent with the male-specific nature of prostate cancer. Preclinical models, including xenografts, patient-derived xenografts, and genetically engineered mouse models (GEMMs), were also male-derived. All prostate cancer cell lines utilized in the study were of male origin, with the exception of Supplementary Figure S5A, where a broader cohort of 1,019 cell lines from the Cancer Cell Line Encyclopedia (CCLE), comprising both male- and

female-derived samples across multiple cancer types, was analyzed. Analyses of CCLE data in Supplementary Figure S5A were performed without stratification by sex.

Transcriptomic data normalization and transcriptome-based signature scores

To ensure consistency and compatibility across diverse datasets, we employed normalization strategies tailored to the specific data types and analytical approaches.

Canonical AR activity score (AR-A), MYC activity score (MYC-sig), and PCa-Stem signature: Canonical pro-differentiation AR-A can be determined by RNA-seq based measurements of AR-regulated transcripts under intact androgen/AR signaling conditions. Similarly, MYC-sig can be determined by MYC-regulated transcripts. We employed Z-score normalization method (72) to determine AR-A and MYC-sig. Briefly, the numeric AR or MYC activity score was calculated based on a linear combination of expression values (Z-scores) of experimentally validated AR targets (14) or MYC targets (51) (Supplementary Table S2, GSEA Molecular Signature Database 2022.1 version, MSigDB). The target gene lists were detailed in Supplementary Table S2. The expression value for each AR or MYC target genes (Supplementary Table S2) was converted to Z-score by $Z = (x - \mu)/\sigma$, where x is the expression value of the target gene in a specific sample, μ is the mean and σ is the standard deviation across all samples of a gene. Finally, the combined Z-scores were summed across all genes to represent the expression score of canonical AR or MYC target genes. Analysis of gene expression signatures using Z-score normalization (AR-A and MYC-sig) was confined within individual datasets, obviating the need for cross-dataset comparisons.

To further minimize batch effects and ensure data integrity and comparability across PCa stages, normalized RNAseq data from a published integrated data framework, the Prostate Cancer Transcriptome Atlas (27) (https://prostatecanceratlas.org), was used. In this harmonized resource, raw RNAseq data with high-quality sequencing reads from different datasets were re-mapped to the human reference genome GRCh38, adjusted for library size, and normalized using the variance stabilizing transformation pipeline using DESeq2 (version 1.28.1; RRID:SCR_015687) (27).

Single-sample gene set enrichment analysis (ssGSEA) was performed using the Gene Set Variation Analysis (GSVA) package (version 1.50.5; RRID:SCR_021058) (73) in R (version 4.3.3; RRID:SCR_001905) to calculate scores for the in-house derived 12-gene PCa-Stem signature (Supplementary Table S2) across different stages of PCa progression using the normalized RNAseq data from the Prostate Cancer Transcriptome Atlas (27).

Transcriptome-based quantitative measurement of oncogenic stemness (the Stemness Index): We adapted mRNA-based Stemness Index (mRNAsi) to determine the degree of oncogenic dedifferentiation (Stemness)(8). Briefly, we computed Spearman correlations between the stemness model's weight vector and the transcriptome expression profile of the queried samples, assuming paired observations, at least ordinal scale data, and a monotonic relationship without significant outliers. Spearman correlation

calculations were performed using the 'stats' package (version 4.3.3) in R (version 4.3.3; RRID:SCR_001905). The resulting correlation coefficients were then linearly transformed to scale the mRNAsi scores between 0 and 1 using the following formula: Stemness Index = (Spearman correlation + 0.2619) /0.4151. Spearman correlation is advocated for calculating the Stemness Index because it is more robust with respect to potential cross-dataset batch effects that may arise (8).

Integrative analysis of genomic alterations in primary PCa (TCGA) and mCRPC (SU2C)

Data on genomic alterations and associated clinical profiles in Pri-PCa (**TCGA-PRAD 2018,** Pan-Cancer Atlas; https://www.cbioportal.org/study/summary?id=prad_tcga_pan_can_atlas_2018) and mCRPC (**SU2C 2019**; https://www.cbioportal.org/study/summary?id=prad_su2c_2019; ref. (41)) were extracted from the cBioPortal for Cancer Genomics (74). Differential expression analysis was performed using DESeq2 (version 1.42.1; RRID:SCR_015687) to identify differentially expressed genes (DEGs) for group comparisons (75).

Statistical analysis

Statistical analyses were performed using GraphPad Prism software (version 10.4.1 (532); RRID:SCR_002798) and R (version 4.3.3; RRID:SCR_001095).

For comparisons between two groups, independent sample or paired *t*-tests were used to compare group means, assuming normality and equal variance. For multiple-group comparisons, Tukey's range test was employed following one-way ANOVA (adjusted p-values are listed in Supplementary Table S4). The Wilcoxon rank-sum test was applied for comparisons of altered genome fraction, tumor mutation burden (TMB), or age between two groups.

For differential expression analyses and comparisons involving multiple hypotheses (e.g., RNAseq-based gene comparisons), p-values were further adjusted using the false discovery rate (FDR) method to control for multiple testing.

Pearson's correlation coefficient was used to evaluate linear associations between two continuous variables, assuming normally distributed paired observations. Linear regression modeling was applied to examine the relationship between two continuous variables, with the slope of the best-fit regression line reported where applicable. Spearman's rank correlation was employed to assess monotonic relationships between continuous or ordinal variables, assuming paired observations and monotonic trends without significant outliers.

The Jonckheere-Terpstra (J-T) trend test was used to assess monotonic association between an ordinal variable and a continuous variable. Chi-square test or Fisher's exact test was performed to evaluate the associations between categorical variables.

For the analysis of patient progression-free survival (PFS) and overall survival (OS), the standard Kaplan-Meier method was used for the estimation of survival fractions and log-rank tests were used for

group comparisons. Cox proportional hazards models were used for multivariable analysis and for assessing the prognostic significance of gene signatures (Stemness, PCa-Stem signature, etc). For the mRNA-based gene signatures (Stemness, PCa-Stem signature, AR-A), patients were stratified into high and low signature groups based on median split in cohorts including Spratt 2017 (Fig. 4C), Tosoian 2020 (Fig. 4C), CHAARTED 2021 (Supplementary Fig. S6C), Taylor 2010 (Supplementary Fig. S6C), TCGA-PRAD 2018 (Supplementary Fig. S6C), and SU2C 2019 (Supplementary Fig. S6C). For certain analyses, including SU2C 2019 (Supplementary Fig. S6C) and CHAARTED 2021 (Fig. 4C), patients were alternatively stratified by comparing the top 25% versus the bottom 75% of signature scores to assess whether patients with very high Stemness levels exhibited a higher risk of disease progression.

All statistical tests were two-sided, and $P < 0.05$ was considered statistically significant.

Data and Code Availability

All datasets and computational codes supporting the findings of this study are described below.

Code Availability: Custom R scripts used for data preprocessing, differential expression analysis, gene signature quantification, and survival/statistical modeling are available from the corresponding author upon reasonable request.

Data Availability: All datasets analyzed in this study are publicly available from repositories including GEO (RRID:SCR_005012), cBioPortal (RRID:SCR_014555), the NCI GDC Portal, Xena Functional Genomics Portal (RRID:SCR_018938), EGA (RRID:SCR_004944), ENA (RRID:SCR_006515), and Zenodo (RRID:SCR_004129), as detailed in Supplementary Table S1.

Authors' Contributions

X. Liu: Conceptualization, data curation, formal analysis, statistical analysis, validation, visualization, investigation, writing–original draft, writing–review and editing, equal contribution as co-first author and co-senior author. **E. Cortes**: Data curation, formal analysis, statistical analysis, validation, investigation, writing–original draft, writing–review and editing, equal contribution as co-first author. **Y. Ji**: Study conception and design, data curation, validation, visualization. **K. Zhao**: Data curation, formal analysis, validation, visualization. **J. Ho**: Data curation, formal analysis, validation, visualization. **Y. Liu**: Data curation, formal analysis, validation, visualization. **E. Davicioni**: Data curation, investigation, writing–review and editing. **F. Feng**: Writing–review and editing. **J. Alumkal**: Writing–review and editing. **D. Spratt**: Writing–review and editing. **C. Sweeney**: Writing–review and editing. **H. Yu**: Data curation, statistical analysis, writing–review and editing. **Q. Hu**: Data curation, statistical analysis, investigation. **Z. Cheng**: Data curation, investigation, writing–review and editing. **D. Zhang**: Data curation, investigation, writing–review and editing. **G. Chatta**: Data curation, investigation, writing–review and editing. **K. Nastiuk**: Data curation, investigation, writing–review and editing. **D. Goodrich**: Obtained main funding for this project, data curation, writing–

review and editing. **K. Rycaj**: Investigation, Data curation, visualization, writing–review and editing. **A. Jamroze**: Investigation, writing–review and editing. **J. Kirk**: Data curation, investigation, writing–original draft, writing–review and editing. **I. Puzanov**: Writing–review and editing. **S. Liu**: Study conception and design, supervision, writing–review and editing, funding acquisition, equal contribution as co-senior author. **J. Wang**: Study conception and design, supervision, writing–review and editing, funding acquisition, equal contribution as co-senior author. **D. Tang**: Conceptualization, supervision, writing–original draft, writing–review and editing, funding acquisition, equal contribution as co-senior author, the lead corresponding author.

Acknowledgements

Work in Tang lab was supported, in part, by grants from the U.S. National Institutes of Health (NIH) National Cancer Institute (NCI) R01CA237027, R01CA240290 and 2R01CA240290-06A1, grants from the U.S. Department of Defense (DOD) PC220137 and PC220273, Roswell Park Comprehensive Cancer Center and the NCI Center grant P30CA016056, Roswell Park Alliance Foundation (RPAF) and the George Decker Endowment. Work in Goodrich lab was support by NIH/NCI R01CA234162 and R01CA230913. Work in the labs of Goodrich, Tang and Chatta was further supported by the Prostate Cancer Foundation (PCF) Challenge Award 2022CHAL3788 (PI: Goodrich). S. Liu and J. Wang were supported by NIH/NCI U24CA232979 and U24CA274159. Work in Alumkal lab was supported by NIH/NCI R01CA251245, PCF Challenge Award, National Comprehensive Cancer Network (NCCN)/Astellas Pharma Global Development Award, Michigan Prostate SPORE (NCI P50 CA186786), and Joint Institute for Translational and Clinical Research. We thank the cloud computing resources provided by the Center for Computational Research (CCR) at the University at Buffalo (http://hdl.handle.net/10477/79221). We thank Mr. W. Tian and Dr. L. Yan for assistance in survival analysis, Drs. J. Yong and H. He for bioinformatics assistance and all other Tang lab members for helpful discussions and suggestions. We apologize to the colleagues whose work was not cited due to space constraint.

References

1. Ben-Porath I, Thomson MW, Carey VJ, Ge R, Bell GW, Regev A, Weinberg RA. An embryonic stem cell-like gene expression signature in poorly differentiated aggressive human tumors. Nat Genet 2008;40(5):499-507 doi 10.1038/ng.127.
2. Pece S, Tosoni D, Confalonieri S, Mazzarol G, Vecchi M, Ronzoni S*, et al.* Biological and molecular heterogeneity of breast cancers correlates with their cancer stem cell content. Cell 2010;140(1):62-73 doi 10.1016/j.cell.2009.12.007.
3. Wong DJ, Liu H, Ridky TW, Cassarino D, Segal E, Chang HY. Module map of stem cell genes guides creation of epithelial cancer stem cells. Cell Stem Cell 2008;2(4):333-44 doi 10.1016/j.stem.2008.02.009.
4. Gupta PB, Pastushenko I, Skibinski A, Blanpain C, Kuperwasser C. Phenotypic Plasticity: Driver of Cancer Initiation, Progression, and Therapy Resistance. Cell Stem Cell 2019;24(1):65-78 doi 10.1016/j.stem.2018.11.011.
5. Loh JJ, Ma S. Hallmarks of cancer stemness. Cell Stem Cell 2024;31(5):617-39 doi 10.1016/j.stem.2024.04.004.
6. Malta TM, Sokolov A, Gentles AJ, Burzykowski T, Poisson L, Weinstein JN*, et al.* Machine Learning Identifies Stemness Features Associated with Oncogenic Dedifferentiation. Cell 2018;173(2):338-54 e15 doi 10.1016/j.cell.2018.03.034.
7. Liu X, Li WJ, Puzanov I, Goodrich DW, Chatta G, Tang DG. Prostate cancer as a dedifferentiated organ: androgen receptor, cancer stem cells, and cancer stemness. Essays Biochem 2022;66(4):291-303 doi 10.1042/EBC20220003.
8. Tang DG. Understanding and targeting prostate cancer cell heterogeneity and plasticity. Semin Cancer Biol 2022;82:68-93 doi 10.1016/j.semcancer.2021.11.001.
9. Siegel RL, Kratzer TB, Giaquinto AN, Sung H, Jemal A. Cancer statistics, 2025. CA Cancer J Clin 2025 75(1):10-45. doi 10.3322/caac.21871.
10. Robinson D, Van Allen EM, Wu YM, Schultz N, Lonigro RJ, Mosquera JM*, et al.* Integrative clinical genomics of advanced prostate cancer. Cell 2015;161(5):1215-28 doi 10.1016/j.cell.2015.05.001.
11. He MX, Cuoco MS, Crowdis J, Bosma-Moody A, Zhang Z, Bi K*, et al.* Transcriptional mediators of treatment resistance in lethal prostate cancer. Nat Med 2021;27(3):426-33 doi 10.1038/s41591-021-01244-6.
12. Westbrook TC, Guan X, Rodansky E, Flores D, Liu CJ, Udager AM*, et al.* Transcriptional profiling of matched patient biopsies clarifies molecular determinants of enzalutamide-induced lineage plasticity. Nat Commun 2022;13(1):5345 doi 10.1038/s41467-022-32701-6.
13. Alumkal JJ, Sun D, Lu E, Beer TM, Thomas GV, Latour E*, et al.* Transcriptional profiling identifies an androgen receptor activity-low, stemness program associated with enzalutamide resistance. Proc Natl Acad Sci U S A 2020;117(22):12315-23 doi 10.1073/pnas.1922207117.
14. Bluemn EG, Coleman IM, Lucas JM, Coleman RT, Hernandez-Lopez S, Tharakan R*, et al.* Androgen Receptor Pathway-Independent Prostate Cancer Is Sustained through FGF Signaling. Cancer Cell 2017;32(4):474-89.e6 doi https://doi.org/10.1016/j.ccell.2017.09.003.
15. Hieronymus H, Lamb J, Ross KN, Peng XP, Clement C, Rodina A*, et al.* Gene expression signature-based chemical genomic prediction identifies a novel class of HSP90 pathway modulators. Cancer Cell 2006;10(4):321-30 doi 10.1016/j.ccr.2006.09.005.

16. Zhang D, Hu Q, Liu X, Ji Y, Chao HP, Liu Y*, et al.* Intron retention is a hallmark and spliceosome represents a therapeutic vulnerability in aggressive prostate cancer. Nat Commun 2020;11(1):2089 doi 10.1038/s41467-020-15815-7.

17. Spratt DE, Alshalalfa M, Fishbane N, Weiner AB, Mehra R, Mahal BA*, et al.* Transcriptomic Heterogeneity of Androgen Receptor Activity Defines a de novo low AR-Active Subclass in Treatment Naive Primary Prostate Cancer. Clin Cancer Res 2019;25(22):6721-30 doi 10.1158/1078-0432.CCR-19-1587.

18. Cancer Genome Atlas Research N. The Molecular Taxonomy of Primary Prostate Cancer. Cell 2015;163(4):1011-25 doi 10.1016/j.cell.2015.10.025.

19. Zhang D, Park D, Zhong Y, Lu Y, Rycaj K, Gong S*, et al.* Stem cell and neurogenic gene-expression profiles link prostate basal cells to aggressive prostate cancer. Nat Commun 2016;7:10798 doi 10.1038/ncomms10798.

20. Smith BA, Sokolov A, Uzunangelov V, Baertsch R, Newton Y, Graim K*, et al.* A basal stem cell signature identifies aggressive prostate cancer phenotypes. Proc Natl Acad Sci U S A 2015;112(47):E6544-52 doi 10.1073/pnas.1518007112.

21. Moad M, Hannezo E, Buczacki SJ, Wilson L, El-Sherif A, Sims D*, et al.* Multipotent Basal Stem Cells, Maintained in Localized Proximal Niches, Support Directed Long-Ranging Epithelial Flows in Human Prostates. Cell Rep 2017;20(7):1609-22 doi 10.1016/j.celrep.2017.07.061.

22. Grossmann S, Hooks Y, Wilson L, Moore L, O'Neill L, Martincorena I*, et al.* Development, maturation, and maintenance of human prostate inferred from somatic mutations. Cell Stem Cell 2021;28(7):1262-74 e5 doi 10.1016/j.stem.2021.02.005.

23. Wyatt AW, Mo F, Wang K, McConeghy B, Brahmbhatt S, Jong L*, et al.* Heterogeneity in the inter-tumor transcriptome of high risk prostate cancer. Genome Biol 2014;15(8):426 doi 10.1186/s13059-014-0426-y.

24. Long X, Hou H, Wang X, Liu S, Diao T, Lai S*, et al.* Immune signature driven by ADT-induced immune microenvironment remodeling in prostate cancer is correlated with recurrence-free survival and immune infiltration. Cell Death Dis 2020;11(9):779 doi 10.1038/s41419-020-02973-1.

25. Rajan P, Sudbery IM, Villasevil ME, Mui E, Fleming J, Davis M*, et al.* Next-generation sequencing of advanced prostate cancer treated with androgen-deprivation therapy. Eur Urol 2014;66(1):32-9 doi 10.1016/j.eururo.2013.08.011.

26. Sharma NV, Pellegrini KL, Ouellet V, Giuste FO, Ramalingam S, Watanabe K*, et al.* Identification of the Transcription Factor Relationships Associated with Androgen Deprivation Therapy Response and Metastatic Progression in Prostate Cancer. Cancers (Basel) 2018;10(10) doi 10.3390/cancers10100379.

27. Bolis M, Bossi D, Vallerga A, Ceserani V, Cavalli M, Impellizzieri D*, et al.* Dynamic prostate cancer transcriptome analysis delineates the trajectory to disease progression. Nat Commun 2021;12(1):7033 doi 10.1038/s41467-021-26840-5.

28. Beltran H, Prandi D, Mosquera JM, Benelli M, Puca L, Cyrta J*, et al.* Divergent clonal evolution of castration-resistant neuroendocrine prostate cancer. Nat Med 2016;22(3):298-305 doi 10.1038/nm.4045.

29. Consortium GT. The Genotype-Tissue Expression (GTEx) project. Nat Genet 2013;45(6):580-5 doi 10.1038/ng.2653.

30. Aran D, Camarda R, Odegaard J, Paik H, Oskotsky B, Krings G*, et al.* Comprehensive analysis of normal adjacent to tumor transcriptomes. Nat Commun 2017;8(1):1077 doi 10.1038/s41467-017-01027-z.

31. Barretina J, Caponigro G, Stransky N, Venkatesan K, Margolin AA, Kim S*, et al.* The Cancer Cell Line Encyclopedia enables predictive modelling of anticancer drug sensitivity. Nature 2012;483(7391):603-7 doi 10.1038/nature11003.

32. Ghandi M, Huang FW, Jane-Valbuena J, Kryukov GV, Lo CC, McDonald ER, 3rd*, et al.* Next-generation characterization of the Cancer Cell Line Encyclopedia. Nature 2019;569(7757):503-8 doi 10.1038/s41586-019-1186-3.

33. Labrecque MP, Coleman IM, Brown LG, True LD, Kollath L, Lakely B*, et al.* Molecular profiling stratifies diverse phenotypes of treatment-refractory metastatic castration-resistant prostate cancer. J Clin Invest 2019;129(10):4492-505 doi 10.1172/JCI128212.

34. Li Q, Deng Q, Chao H-P, Liu X, Lu Y, Lin K*, et al.* Linking prostate cancer cell AR heterogeneity to distinct castration and enzalutamide responses. Nature communications 2018;9(1):1-17.

35. Weiner AB, Liu Y, Hakansson A, Zhao X, Proudfoot JA, Ho J*, et al.* A novel prostate cancer subtyping classifier based on luminal and basal phenotypes. Cancer 2023;129(14):2169-78 doi 10.1002/cncr.34790.

36. Taylor BS, Schultz N, Hieronymus H, Gopalan A, Xiao Y, Carver BS*, et al.* Integrative genomic profiling of human prostate cancer. Cancer Cell 2010;18(1):11-22 doi 10.1016/j.ccr.2010.05.026.

37. Ku SY, Rosario S, Wang Y, Mu P, Seshadri M, Goodrich ZW*, et al.* Rb1 and Trp53 cooperate to suppress prostate cancer lineage plasticity, metastasis, and antiandrogen resistance. Science 2017;355(6320):78-83 doi 10.1126/science.aah4199.

38. Spratt DE, Yousefi K, Deheshi S, Ross AE, Den RB, Schaeffer EM*, et al.* Individual Patient-Level Meta-Analysis of the Performance of the Decipher Genomic Classifier in High-Risk Men After Prostatectomy to Predict Development of Metastatic Disease. J Clin Oncol 2017;35(18):1991-8 doi 10.1200/JCO.2016.70.2811.

39. Tosoian JJ, Birer SR, Jeffrey Karnes R, Zhang J, Davicioni E, Klein EE*, et al.* Performance of clinicopathologic models in men with high risk localized prostate cancer: impact of a 22-gene genomic classifier. Prostate Cancer Prostatic Dis 2020;23(4):646-53 doi 10.1038/s41391-020-0226-2.

40. Hamid AA, Huang HC, Wang V, Chen YH, Feng F, Den R*, et al.* Transcriptional profiling of primary prostate tumor in metastatic hormone-sensitive prostate cancer and association with clinical outcomes: correlative analysis of the E3805 CHAARTED trial. Ann Oncol 2021;32(9):1157-66 doi 10.1016/j.annonc.2021.06.003.

41. Abida W, Cyrta J, Heller G, Prandi D, Armenia J, Coleman I*, et al.* Genomic correlates of clinical outcome in advanced prostate cancer. Proc Natl Acad Sci U S A 2019;116(23):11428-36 doi 10.1073/pnas.1902651116.

42. Zhao SG, Chang SL, Erho N, Yu M, Lehrer J, Alshalalfa M*, et al.* Associations of Luminal and Basal Subtyping of Prostate Cancer With Prognosis and Response to Androgen Deprivation Therapy. JAMA Oncol 2017;3(12):1663-72 doi 10.1001/jamaoncol.2017.0751.

43. Zhao SG, Chen WS, Das R, Chang SL, Tomlins SA, Chou J*, et al.* Clinical and Genomic Implications of Luminal and Basal Subtypes Across Carcinomas. Clin Cancer Res 2019;25(8):2450-7 doi 10.1158/1078-0432.CCR-18-3121.

44. Coleman IM, DeSarkar N, Morrissey C, Xin L, Roudier MP, Sayar E*, et al.* Therapeutic Implications for Intrinsic Phenotype Classification of Metastatic Castration-Resistant Prostate Cancer. Clin Cancer Res 2022;28(14):3127-40 doi 10.1158/1078-0432.CCR-21-4289.

45. You S, Knudsen BS, Erho N, Alshalalfa M, Takhar M, Al-Deen Ashab H*, et al.* Integrated Classification of Prostate Cancer Reveals a Novel Luminal Subtype with Poor Outcome. Cancer Res 2016;76(17):4948-58 doi 10.1158/0008-5472.CAN-16-0902.

905 46. Yoon J, Kim M, Posadas EM, Freedland SJ, Liu Y, Davicioni E*, et al.* A comparative study of PCS
906 and PAM50 prostate cancer classification schemes. Prostate Cancer Prostatic Dis
907 2021;24(3):733-42 doi 10.1038/s41391-021-00325-4.

908 47. Jamroze A, Liu X, Tang DG. Treatment-induced stemness and lineage plasticity in driving
909 prostate cancer therapy resistance. Cancer Heterogeneity and Plasticity 2024;1(1) doi
910 10.47248/chp2401010005.

911 48. Tang F, Xu D, Wang S, Wong CK, Martinez-Fundichely A, Lee CJ*, et al.* Chromatin profiles
912 classify castration-resistant prostate cancers suggesting therapeutic targets. Science
913 2022;376(6596):eabe1505 doi 10.1126/science.abe1505.

914 49. Armenia J, Wankowicz SAM, Liu D, Gao J, Kundra R, Reznik E*, et al.* The long tail of oncogenic
915 drivers in prostate cancer. Nat Genet 2018;50(5):645-51 doi 10.1038/s41588-018-0078-z.

916 50. Haffner MC, Zwart W, Roudier MP, True LD, Nelson WG, Epstein JI*, et al.* Genomic and
917 phenotypic heterogeneity in prostate cancer. Nat Rev Urol 2021;18(2):79-92 doi 10.1038/s41585-
918 020-00400-w.

919 51. Liberzon A, Birger C, Thorvaldsdottir H, Ghandi M, Mesirov JP, Tamayo P. The Molecular
920 Signatures Database (MSigDB) hallmark gene set collection. Cell Syst 2015;1(6):417-25 doi
921 10.1016/j.cels.2015.12.004.

922 52. Tomlins SA, Mehra R, Rhodes DR, Cao X, Wang L, Dhanasekaran SM, et al. Integrative
923 molecular concept modeling of prostate cancer progression. Nat Genet 2007;39(1):41-51 doi
924 10.1038/ng1935.

925 53. Stuchbery R, Macintyre G, Cmero M, Harewood LM, Peters JS, Costello AJ*, et al.* Reduction in
926 expression of the benign AR transcriptome is a hallmark of localised prostate cancer progression.
927 Oncotarget 2016;7(21):31384-92 doi 10.18632/oncotarget.8915.

928 54. Schroeder A, Herrmann A, Cherryholmes G, Kowolik C, Buettner R, Pal S*, et al.* Loss of
929 androgen receptor expression promotes a stem-like cell phenotype in prostate cancer through
930 STAT3 signaling. Cancer Res 2014;74(4):1227-37 doi 10.1158/0008-5472.CAN-13-0594.

931 55. Giridhar PV, Williams K, VonHandorf AP, Deford PL, Kasper S. Constant degradation of the
932 androgen receptor by MDM2 conserves prostate cancer stem cell integrity. Cancer research
933 2019;79(6):1124-37.

934 56. Liu X, Grogan TR, Hieronymus H, Hashimoto T, Mottahedeh J, Cheng D*, et al.* Low CD38
935 Identifies Progenitor-like Inflammation-Associated Luminal Cells that Can Initiate Human Prostate
936 Cancer and Predict Poor Outcome. Cell Rep 2016;17(10):2596-606 doi
937 10.1016/j.celrep.2016.11.010.

938 57. Kirk JS, Wang J, Long M, Rosario S, Tracz A, Ji Y*, et al.* Integrated single-cell analysis defines
939 the epigenetic basis of castration-resistant prostate luminal cells. Cell Stem Cell 2024 doi
940 10.1016/j.stem.2024.05.008.

941 58. Gulati GS, Sikandar SS, Wesche DJ, Manjunath A, Bharadwaj A, Berger MJ*, et al.* Single-cell
942 transcriptional diversity is a hallmark of developmental potential. Science 2020;367(6476):405-11
943 doi 10.1126/science.aax0249.

944 59. Chauhan PS, Alahi I, Sinha S, Ledet EM, Mueller R, Linford J*, et al.* Genomic and Epigenomic
945 Analysis of Plasma Cell-Free DNA Identifies Stemness Features Associated with Worse Survival
946 in Lethal Prostate Cancer. Clin Cancer Res 2025;31(1):151-63 doi 10.1158/1078-0432.CCR-24-
947 1658.

948 60. Liu J, Lichtenberg T, Hoadley KA, Poisson LM, Lazar AJ, Cherniack AD*, et al.* An Integrated
949 TCGA Pan-Cancer Clinical Data Resource to Drive High-Quality Survival Outcome Analytics. Cell
950 2018;173(2):400-16 e11 doi 10.1016/j.cell.2018.02.052.

951 61. Jamroze A, Zhang R, Deng L, Jatwani K, Nguyen U, Farmer B*, et al.* Neoadjuvant androgen
952 deprivation therapy initially activates and subsequently suppresses the prostate cancer tumor
953 immune microenvironment (Submitted 2024).

954 62. Gerhauser C, Favero F, Risch T, Simon R, Feuerbach L, Assenov Y*, et al.* Molecular Evolution of
955 Early-Onset Prostate Cancer Identifies Molecular Risk Markers and Clinical Trajectories. Cancer
956 Cell 2018;34(6):996-1011 e8 doi 10.1016/j.ccell.2018.10.016.

957 63. Suntsova M, Gaifullin N, Allina D, Reshetun A, Li X, Mendeleeva L*, et al.* Atlas of RNA
958 sequencing profiles for normal human tissues. Sci Data 2019;6(1):36 doi 10.1038/s41597-019-
959 0043-4.

960 64. Stelloo S, Nevedomskaya E, Kim Y, Schuurman K, Valle-Encinas E, Lobo J*, et al.* Integrative
961 epigenetic taxonomy of primary prostate cancer. Nat Commun 2018;9(1):4900 doi
962 10.1038/s41467-018-07270-2.

963 65. Ramnarine VR, Alshalalfa M, Mo F, Nabavi N, Erho N, Takhar M*, et al.* The long noncoding RNA
964 landscape of neuroendocrine prostate cancer and its clinical implications. Gigascience 2018;7(6)
965 doi 10.1093/gigascience/giy050.

966 66. Robinson DR, Wu YM, Lonigro RJ, Vats P, Cobain E, Everett J*, et al.* Integrative clinical
967 genomics of metastatic cancer. Nature 2017;548(7667):297-303 doi 10.1038/nature23306.

968 67. Sharp A, Coleman I, Yuan W, Sprenger C, Dolling D, Rodrigues DN*, et al.* Androgen receptor
969 splice variant-7 expression emerges with castration resistance in prostate cancer. J Clin Invest
970 2019;129(1):192-208 doi 10.1172/JCI122819.

971 68. Nyquist MD, Corella A, Coleman I, De Sarkar N, Kaipainen A, Ha G*, et al.* Combined TP53 and
972 RB1 Loss Promotes Prostate Cancer Resistance to a Spectrum of Therapeutics and Confers
973 Vulnerability to Replication Stress. Cell Rep 2020;31(8):107669 doi
974 10.1016/j.celrep.2020.107669.

975 69. Brady L, Kriner M, Coleman I, Morrissey C, Roudier M, True LD*, et al.* Inter- and intra-tumor
976 heterogeneity of metastatic prostate cancer determined by digital spatial gene expression
977 profiling. Nat Commun 2021;12(1):1426 doi 10.1038/s41467-021-21615-4.

978 70. Lim Y, Arora S, Schuster SL, Corey L, Fitzgibbon M, Wladyka CL*, et al.* Multiplexed functional
979 genomic analysis of 5' untranslated region mutations across the spectrum of prostate cancer. Nat
980 Commun 2021;12(1):4217 doi 10.1038/s41467-021-24445-6.

981 71. Goldman MJ, Craft B, Hastie M, Repecka K, McDade F, Kamath A, et al. Visualizing and
982 interpreting cancer genomics data via the Xena platform. Nat Biotechnol 2020;38(6):675-8 doi
983 10.1038/s41587-020-0546-8.

984 72. Lee E, Chuang HY, Kim JW, Ideker T, Lee D. Inferring pathway activity toward precise disease
985 classification. PLoS Comput Biol 2008;4(11):e1000217 doi 10.1371/journal.pcbi.1000217.

986 73. Hanzelmann S, Castelo R, Guinney J. GSVA: gene set variation analysis for microarray and
987 RNA-seq data. BMC Bioinformatics 2013;14:7 doi 10.1186/1471-2105-14-7.

988 74. Gao J, Aksoy BA, Dogrusoz U, Dresdner G, Gross B, Sumer SO*, et al.* Integrative analysis of
989 complex cancer genomics and clinical profiles using the cBioPortal. Sci Signal 2013;6(269):pl1
990 doi 10.1126/scisignal.2004088.

991 75. Love MI, Huber W, Anders S. Moderated estimation of fold change and dispersion for RNA-seq
992 data with DESeq2. Genome Biol 2014;15(12):550 doi 10.1186/s13059-014-0550-8.

993

Figure Legends

Figure 1. *Pri-PCa shows concordant increases of AR-A and Stemness and both are decreased by nADT.*
A-C, PCa has increased AR-A as well as the Stemness compared to matched benign tissues. Pairwise comparisons of *AR* mRNA levels, canonical AR-A, and Stemness scores showing significant increases in primary tumors (T) as compared to the matched adjacent benign prostate tissues (N) from the same individual in TCGA-PRAD cohort (n=51; **A**), and Wyatt 2014 cohort (n=12; **B**). In the Long 2020 cohort (n=10; **C**), increases in AR-A and Stemness reached statistical significance whereas the increase in *AR* mRNA levels approached statistical significance ($P = 0.06$).
D-F, nADT decreases both AR-A and Stemness. Pairwise comparison of *AR* mRNA levels, AR-A, and Stemness showing significant decrease of both AR-A and Stemness after nADT (Post-nADT) as compared to the matched samples before nADT (Pre-nADT) from the same individual (**D**, Rajan 2014 cohort; **E**, Sharma 2018 cohort; **F**, Long 2020 cohort).
In all plots, sample sizes are indicated (see also Supplementary Table S1 for cohort and RNA-seq data access information). Within the plots, results are shown as the mean ± SD and pairs are linked with a grey line. Significance was calculated by two-tailed paired Student's *t*-test (ns, not significant; *, $P < 0.05$; **, $P < 0.01$; ***, $P < 0.001$; ****, $P < 0.0001$).

Figure 2. *Continual increases in Stemness with declining AR-A during spontaneous PCa progression*.
A, The pie chart showing sample sizes in different Gleason grades in the TCGA untreated Pri-PCa cohort.
B-D, Progression of treatment-naïve Pri-PCa is accompanied by decreasing AR-A but increasing Stemness. Data is presented as mean ± SD. Shown on top are the Jonckheere-Terpstra's trend (J-T) test results (wedges).
E-F, Progression in Pri-PCa is accompanied by a gradual loss of the positive correlation between canonical AR-A and Stemness. Scatter plots illustrating the correlation between AR-A and Stemness in (**E**) combined Pri-PCa cases in TCGA with an overall linear regression model and (**F**) individual GS grades with corresponding linear regressions showing decreasing slopes from low to high GS grades by J-T test. The slopes of best-fit regression line are also shown.
G, Merged scatter plot showing the correlation between AR-A and Stemness across the 4 GS PCa with each GS represented by a distinct color. The correlation becomes progressively weaker from GS6 to GS9/10, transitioning from positive to nearly zero. The correlation coefficients (r) and p-values for each GS are as follows: GS6 ($r = 0.56$, $P < 0.0001$), GS7 ($r = 0.37$, $P < 0.0001$), GS8 ($r = 0.48$, $P = 0.022$), and GS9/10 ($r = -0.02$, $P = 0.89$). Linear regression lines are overlaid for each GS, demonstrating the decline in the correlation co-efficiency as the GS increases.
All statistical analyses were performed using R and statistical significance was assessed using one-way analysis of variance followed by Tukey's multiple-comparison test (B-D). J-T trend test in B-D and F was used to calculate the statistical significance of the trend across different groups. *, $P < 0.05$; **, $P < 0.01$; ***, $P < 0.001$; ****, $P < 0.0001$; ns, not significant.

Figure 3. *Therapies and metastatic progression drive further divergence between Stemness and canonical AR-A with mCRPC showing the highest Stemness but the lowest AR-A*.
A-D, Hormonal treatment further drives down AR-A but significantly upregulates Stemness. **A-C**, mCRPC displays the lowest pro-differentiation AR-A but highest Stemness. Shown are *AR* mRNA levels (**A**), the canonical AR-A (**B**) and Stemness (**C**) in tumor-adjacent benign tissues (N), treatment-naïve Pri-PCa and advanced Pri-PCa with post-surgery adjuvant ADT (Tx) in TCGA, and mCRPC (SU2C 2015). Sample sizes are indicated in parentheses. Shown on top are the Jonckheere-Terpstra's (J-T) trend test results (wedges). **D,** Stemness inversely correlates with AR-A in mCRPC**.** Shown are scatter plots with best-fit linear regression lines illustrating the correlation between AR-A and Stemness with Pearson correlation coefficient (r), the slopes of lines and J-T test results of slopes indicated below.
E-F, PCa progression is accompanied by loss of AR-A (**E**) but gain of Stemness (**F**) across PCa states. Shown are samples representing the spectrum of PCa development and progression, from normal (organ

donors in GTEx) to (tumor-adjacent) benign tissues, to (treatment-naïve) Pri-PCa, aggressive Pri-PCa treated with adjuvant ADT (Pri-PCa/ADT), mCRPC, and, finally, to (clonally-derived) PCa models including PDX, xenografts and cells lines. From Left to right: Normal (n=116): Normal prostates from GTEx; Benign (n=52): tumor-adjacent benign tissue from TCGA-PRAD; Pri-PCa (n=422): treatment-naïve localized PCa from TCGA-PRAD; Pri-PCa/ADT (n=70): advanced Pri-PCa treated with adjuvant hormone therapy from TCGA-PRAD; mCRPC (n=59): mCRPC from GSE126078; mCRPC (n=135): mCRPC from SU2C 2015 cohort; mCRPC-Adeno (n=34): adenocarcinoma mCRPC from Beltran 2016 cohort; mCRPC-NE (n=15): neuroendocrine mCRPC from Beltran 2016 cohort; mCRPC (n=42): mCRPC from Westbrook 2022; mCRPC (n=25): mCRPC from Alumkal 2020; PDX-LuCaP (n=39): PCa PDXs from GSE126078; PCa cell lines (n=8): PCa cell lines from CCLE; XG-LAPC9 (n=10) and XG-LNCaP (n=12): PCa xenografts from GSE88752. Statistical significances between groups were shown in inverted pyramid grid plot as indicated by different colors. Student's *t*-test was used to compare each group and adjusted p-value for multiple comparisons was done by Tukey's range test. See Supplementary Table S4 for the summary of statistical comparisons. J-T trend test was used to assess the statistical significance of the trend across groups. See also Supplementary Table S1 for cohort and RNA-seq data access information.

G, Scatter plots in the Bolis 2021 integrated cohort (normal n=174, Pri-PCa n=714, mCRPC n=335) showing the changing correlation between AR-A and Stemness across disease stages: positive in normal to weaker correlations in Pri-PCa to negative correlations in mCRPC. Regression lines are color-coded, and the slope of the best-fit regression line and Pearson's r are provided: yellow for normal (Pearson's r=0.42, P <0.0001; slope: 43.87, 95%CI, 29.57 to 58.18); blue for Pri-PCa (r=0.32, P <0.0001; slope: 15.04, 95%CI, 11.76 to 18.32); and green for mCRPC (r=-0.15, P = 0.005; slope: -17.25, 95%CI, -29.24 to -5.26).

H, Violin plot showing increasing Stemness among the NCCN Risk Groups containing 82470 microarray samples with localized disease in GRID. J-T trend test was used to assess the statistical significance of the trend across groups.

I-M, Increasing Stemness during PCa progression in the Taylor 2010 cohort consisting of tumor-adjacent benign tissue (Normal; n=29), Pri-PCa (n=131) and metastatic mPCa (n=19). The AR-A significantly increased in Pri-PCa vs. Normal and significantly decreased in mPCa compared to Pri-PCa (**I**) whereas the Stemness continued to increase from Benign to Pri-PCa to mPCa (**J**). **K-M**, Scatter plots illustrating the correlations between AR-A and Stemness in different contexts with corresponding linear regression lines: **K,** Positive correlation in normal (Pearson's r=0.69, P <0.0001); **L,** a gradual loss of positive correlation between Stemness and AR-A during PCa progression (Pearson's r=0.18, P = 0.043); **M,** a loss of positive correlation between the Stemness and AR-A at more advanced mPCa stage (Pearson's r=0.18, P =0.47).

All data in dot plots and violin plots are shown as mean ± SD. Statistical significance was determined using one-way analysis of variance (ANOVA) followed by Tukey's multiple-comparison test. Jonckheere-Terpstra's trend (J-T) test was used to calculate the statistical significance of the trend across different groups. Pearson correlation coefficients (Pearson's r) were used to calculate the correlations between the Stemness and AR-A. Note: ns, not significant; *, P < 0.05; **, P < 0.01; ***, P < 0.001; ****, P < 0.0001.

Figure 4. *High Stemness is associated with poor patient overall survival.*

A-C, Kaplan-Meier plots showing that high Stemness associates with worse overall survival in PCa patients from Spratt 2017 (**A**), Tosoian 2020 (**B**), and CHAARTED 2021 (**C**) cohorts. P value was determined using the log-rank test.

D, Stemness increases across patient groups with higher Decipher genomic classifier scores. The three cohorts were arranged by their median Decipher genomic classifier scores, and the J-T trend test was used to assess statistical significance of this trend.

Figure 5. *Stemness-high PCa are associated with aggressive molecular subtypes and a 12-gene PCa-stem signature prognosticates poor patient survival.*

A, Schematic illustrating the profiling strategy used to assess associations between Stemness and molecular features in PCa. Patients were ranked by Stemness score and stratified into Stemness-high (top 33%) and Stemness-low (bottom 33%) groups for downstream analyses. Genome-wide functional analyses were performed using transcriptomic, genomic, and clinical data.

B-C, Volcano plots showing differentially expressed genes (DEGs) between Stemness-high and Stemness-low groups in Pri-PCa (**B**) and mCRPC (**C**) cohorts. Red and blue indicate upregulated and downregulated DEGs, respectively. Genes with FDR > 0.05 are shown in gray. Sample sizes (n) of each group are indicated. See Supplementary Table S3 for complete DEG lists.

D Venn diagram showing the 12-gene 'PCa-Stem signature' derived from overlapping upregulated DEGs (FC ≥ 2, FDR < 0.05) in both Pri-PCa and mCRPC.

E-F, GSEA showing low Stemness is associated with immune signaling and inflammatory response (**E**) while high Stemness in both cohorts is enriched for embryonic stem cell traits, aggressiveness, DNA repair, MYC activation, and mTORC1 signaling (**F**). All enrichments are significant ($P < 0.05$, FDR < 0.05).

G-H, PAM50 subtyping showing a higher frequency of LumB subtype in Stemness-high versus Stemness-low samples in Pri-PCa (**G**) and mCRPC (**H**). (****, $P < 0.0001$, χ^2 test).

I-L, GSEA showing enrichment of the aggressive PCS1 gene expression signature in Stemness-high groups and the less aggressive PCS3 signature in Stemness-low groups in Pri-PCa (**I**, **K**) and mCRPC (**J**, **L**). The Prostate Cancer Subtype (PCS) classification system (45,46) stratifies tumors into three molecular subtypes based on transcriptomic features: PCS1 (most aggressive), PCS2 (intermediate), and PCS3 (least aggressive). See Supplementary Table S2 for PCS gene signature.

M-R, GSEA showing AR signature enrichment in Pri-PCa Stemness-high (**M**), NEPC signature enrichment in mCRPC Stemness-high (**N**), and shared enrichment of cell cycle (**O**, **P**) and lineage plasticity (**Q**, **R**) programs in both cohorts. See Supplementary Table S5 for gene sets.

S-V, Kaplan-Meier analyses showing that the 12-gene PCa-Stem signature predicts worse progression-free survival (PFS) in TCGA Pri-PCa (**S**) and worse overall survival (OS) in SU2C mCRPC (**U**). Multivariable Cox models adjusting for clinicopathologic variables confirm the PCa-Stem-High subgroup as independently prognostic for PFS (**T**) and OS (**V**).

Figure 6. *Stemness-high PCa is associated with higher genomic instability.*

A-C, Box plots showing that Stemness-high subgroup in both Pri-PCa (n = 141) and mCRPC (n = 89) displays a higher fraction of altered genome (**A**), higher TMB (**B**), and no age difference compared to Stemness-low cases (**C**). Wilcoxon rank-sum test was used to determine significance (****, $P < 0.0001$; ns, not significant). Statistical significance was determined using the two-sided Wilcoxon rank-sum test. Box plots represent the median, interquartile range (IQR), and whiskers extending to 1.5× the IQR.

D-F, Comparisons of genomic alteration frequencies (Alt. Freq) in cancer-associated genes between Stemness-high and Stemness-low subgroups in TCGA Pri-PCa (**D**, **F**) and SU2C mCRPC (**E**, **F**) cohorts. Statistical significance was determined by two-sided Fisher's Exact test (*, $P < 0.05$).

Figure 7. *MYC activation contributes to increased Stemness during spontaneous PCa progression.*

A-B, Pairwise comparisons showing increased *MYC* mRNA levels and MYC activity (MYC-sig) in primary tumors (T) versus matched adjacent benign tissues (N) in TCGA-PRAD cohort (n=51; **A**) and Wyatt (n=12; **B**) cohorts. Data is shown as mean ± SD; paired samples are linked by grey lines. Significance was determined using two-tailed paired Student's *t*-test (****, $P < 0.0001$).

C-H, MYC activity increases during PCa progression, peaking in mCRPC. In treatment-naïve Pri-PCa (**C**), MYC-sig is significantly increased in all-grade (GS) tumors as compared to tumor-adjacent benign

tissues (N) with the most advanced GS9/10 tumors exhibiting the highest MYC-sig. In **D**, MYC-sig increases from normal to treatment-naïve Pri-PCa and further in advanced Pri-PCa treated with adjuvant ADT (Tx) in TCGA-PRAD, while mCRPC shows the highest MYC-sig in both SU2C 2015 (**D**) and Taylor 2010 (**E**) cohorts. Data is presented as mean ± SD. Statistical significance was assessed by one-way ANOVA with Tukey's multiple-comparison test (**C-E**). J-T trend test was used in (C, D) to assess the significance of progressive increase. **, $P < 0.01$; ***, $P < 0.001$; ****, $P < 0.0001$; ns, not significant. **F-H,** Scatter plots showing positive correlations between MYC activity and Stemness in the Taylor 2010 cohort across different stages. Pearson's r and P-values are indicated.

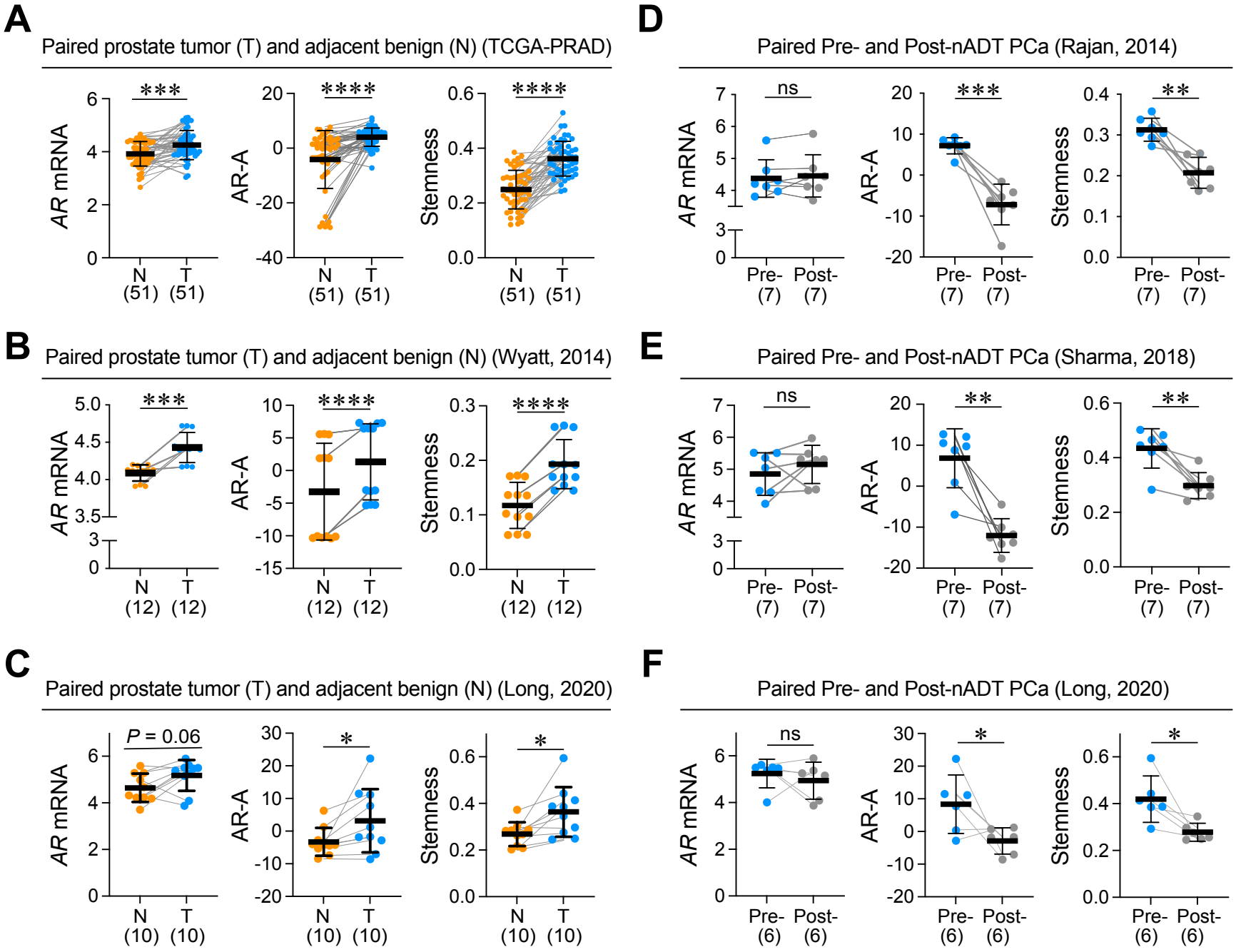
A
Paired prostate tumor (T) and adjacent benign (N) (TCGA-PRAD)
AR mRNA
AR-A
Stemness
***
****
****
N (51)
T (51)
B
Paired prostate tumor (T) and adjacent benign (N) (Wyatt, 2014)
***
****
****
N (12)
T (12)
C
Paired prostate tumor (T) and adjacent benign (N) (Long, 2020)
P = 0.06
*
*
N (10)
T (10)
D
Paired Pre- and Post-nADT PCa (Rajan, 2014)
ns
***
**
Pre- (7)
Post- (7)
E
Paired Pre- and Post-nADT PCa (Sharma, 2018)
ns
**
**
Pre- (7)
Post- (7)
F
Paired Pre- and Post-nADT PCa (Long, 2020)
ns
*
*
Pre- (6)
Post- (6)

Figure 1

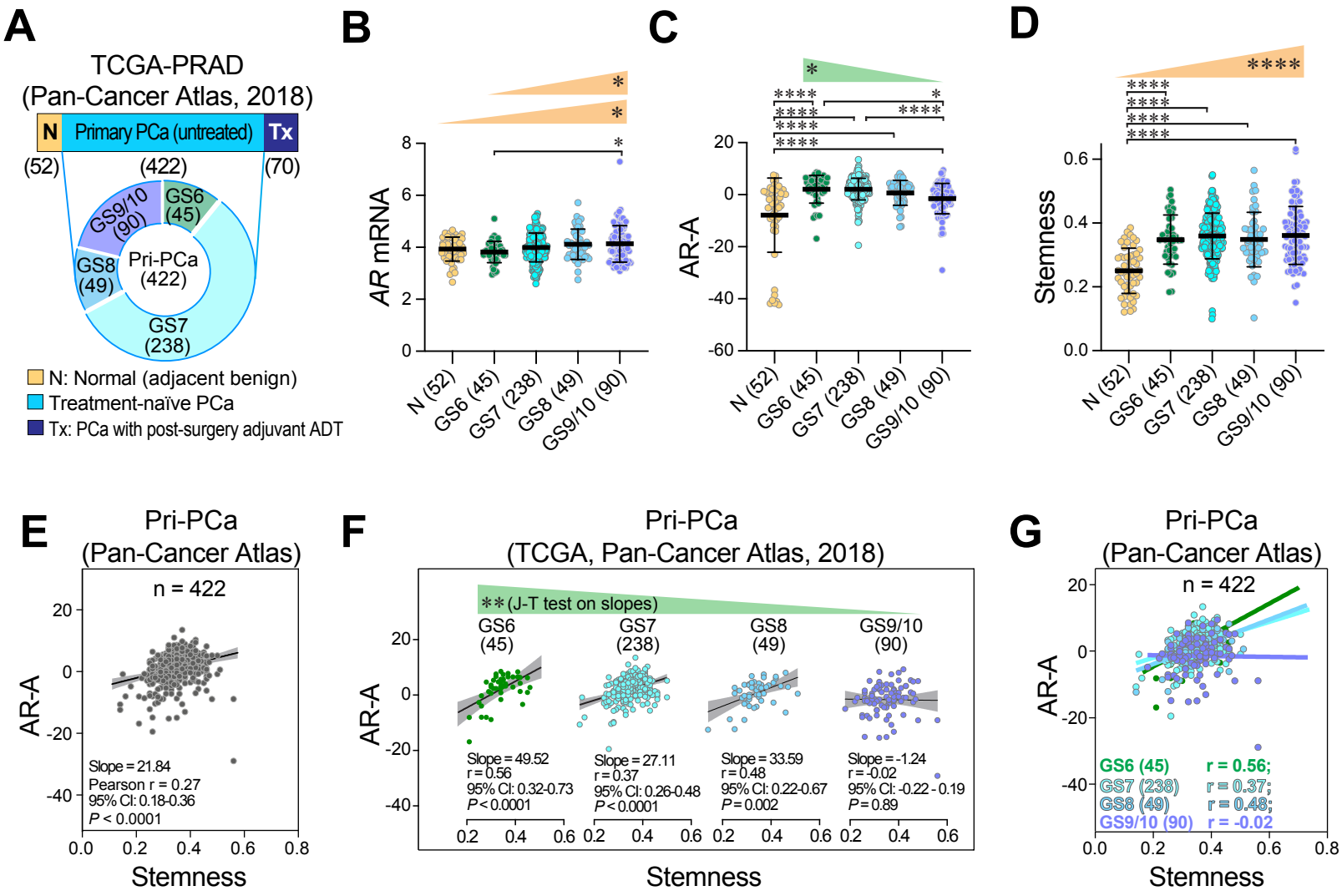
A
TCGA-PRAD
(Pan-Cancer Atlas, 2018)
N
Primary PCa (untreated)
Tx
(52)
(422)
(70)
GS9/10 (90)
GS6 (45)
GS8 (49)
Pri-PCa (422)
GS7 (238)
N: Normal (adjacent benign)
Treatment-naïve PCa
Tx: PCa with post-surgery adjuvant ADT
B
AR mRNA
N (52)
GS6 (45)
GS7 (238)
GS8 (49)
GS9/10 (90)
C
AR-A
D
Stemness
E
Pri-PCa
(Pan-Cancer Atlas)
n = 422
AR-A
Slope = 21.84
Pearson r = 0.27
95% CI: 0.18-0.36
P < 0.0001
Stemness
F
Pri-PCa
(TCGA, Pan-Cancer Atlas, 2018)
** (J-T test on slopes)
GS6 (45)
GS7 (238)
GS8 (49)
GS9/10 (90)
Slope = 49.52
r = 0.56
95% CI: 0.32-0.73
P < 0.0001
Slope = 27.11
r = 0.37
95% CI: 0.26-0.48
P < 0.0001
Slope = 33.59
r = 0.48
95% CI: 0.22-0.67
P = 0.002
Slope = -1.24
r = -0.02
95% CI: -0.22 - 0.19
P = 0.89
Stemness
G
Pri-PCa
(Pan-Cancer Atlas)
n = 422
AR-A
GS6 (45) r = 0.56;
GS7 (238) r = 0.37;
GS8 (49) r = 0.48;
GS9/10 (90) r = -0.02
Stemness

Figure 2

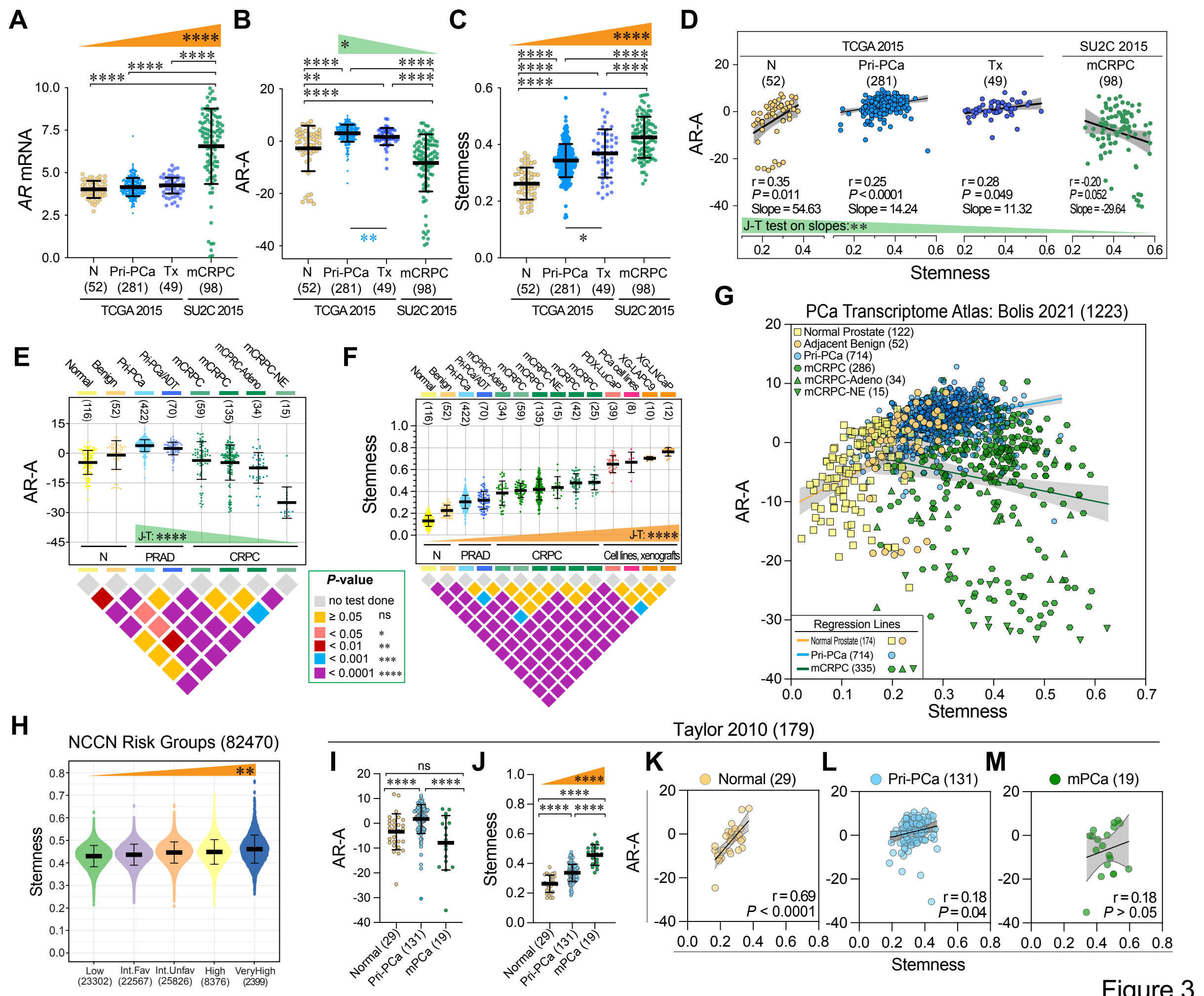
A
AR mRNA
N (52)
Pri-PCa (281)
Tx (49)
mCRPC (98)
TCGA 2015
SU2C 2015
B
AR-A
C
Stemness
D
TCGA 2015
SU2C 2015
r = 0.35
P = 0.011
Slope = 54.63
r = 0.25
P < 0.0001
Slope = 14.24
r = 0.28
P = 0.049
Slope = 11.32
r = -0.20
P = 0.052
Slope = -29.64
J-T test on slopes: **
E
Normal
Benign
Pri-PCa
Pri-PCa/ADT
mCRPC
mCRPC
mCRPC-Adeno
mCRPC-NE
J-T: ****
N
PRAD
CRPC
P-value
no test done
≥ 0.05 ns
< 0.05 *
< 0.01 **
< 0.001 ***
< 0.0001 ****
F
Cell lines, xenografts
G
PCa Transcriptome Atlas: Bolis 2021 (1223)
Normal Prostate (122)
Adjacent Benign (52)
Pri-PCa (714)
mCRPC (286)
mCRPC-Adeno (34)
mCRPC-NE (15)
Regression Lines
Normal Prostate (174)
Pri-PCa (714)
mCRPC (335)
H
NCCN Risk Groups (82470)
Low (23302)
Int.Fav (22567)
Int.Unfav (25826)
High (8376)
VeryHigh (2399)
Taylor 2010 (179)
I
J
K
Normal (29)
L
Pri-PCa (131)
M
mPCa (19)
r = 0.69
P < 0.0001
r = 0.18
P = 0.04
r = 0.18
P > 0.05

Figure 3

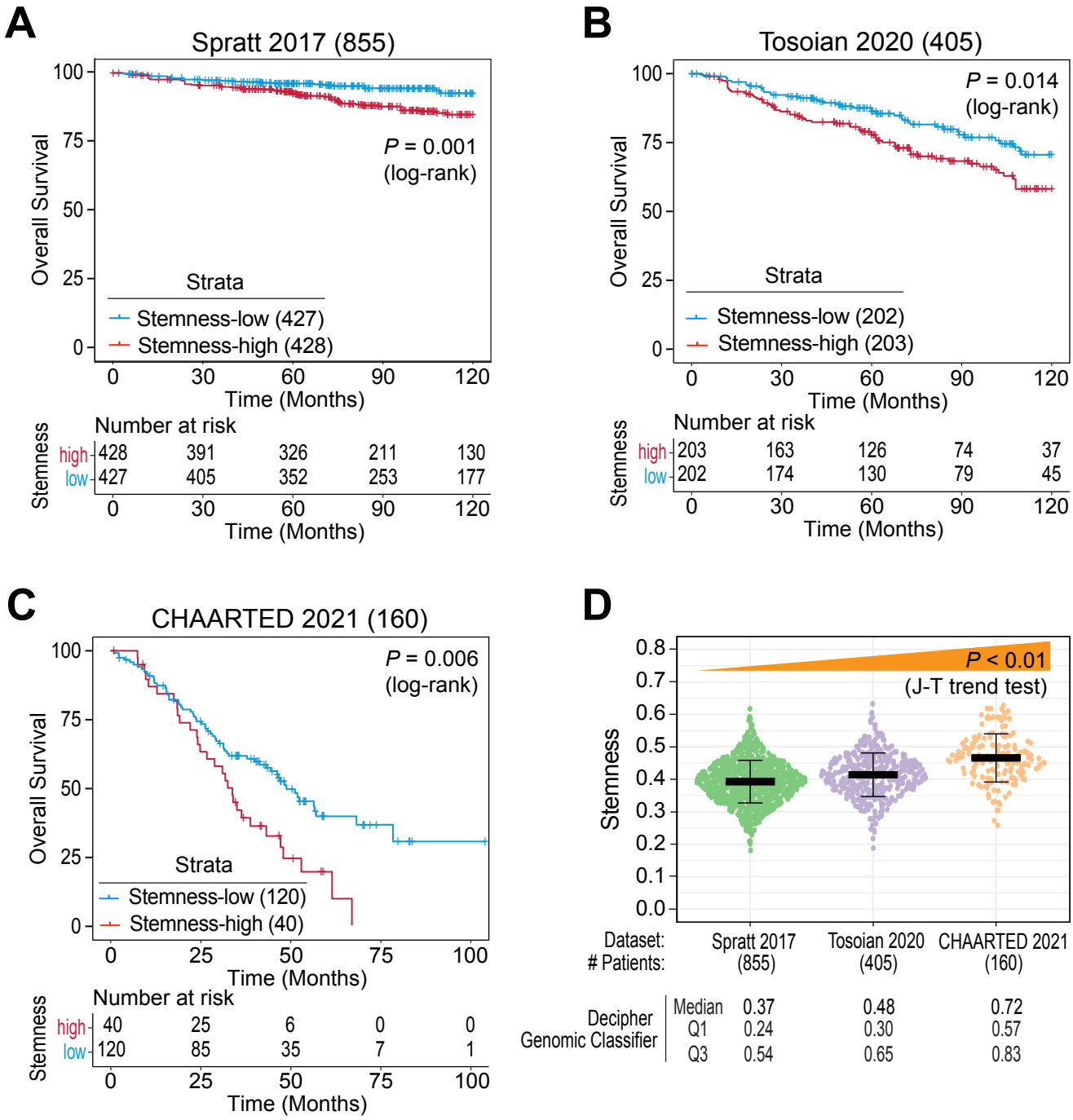
A
Spratt 2017 (855)
Overall Survival
P = 0.001
(log-rank)
Strata
Stemness-low (427)
Stemness-high (428)
Time (Months)
Number at risk
Stemness
high 428 391 326 211 130
low 427 405 352 253 177
B
Tosoian 2020 (405)
P = 0.014
(log-rank)
Stemness-low (202)
Stemness-high (203)
high 203 163 126 74 37
low 202 174 130 79 45
C
CHAARTED 2021 (160)
P = 0.006
(log-rank)
Stemness-low (120)
Stemness-high (40)
high 40 25 6 0 0
low 120 85 35 7 1
D
P < 0.01
(J-T trend test)
Stemness
Dataset:
Patients:
Spratt 2017 (855)
Tosoian 2020 (405)
CHAARTED 2021 (160)
Decipher Genomic Classifier
Median 0.37 0.48 0.72
Q1 0.24 0.30 0.57
Q3 0.54 0.65 0.83

Figure 4

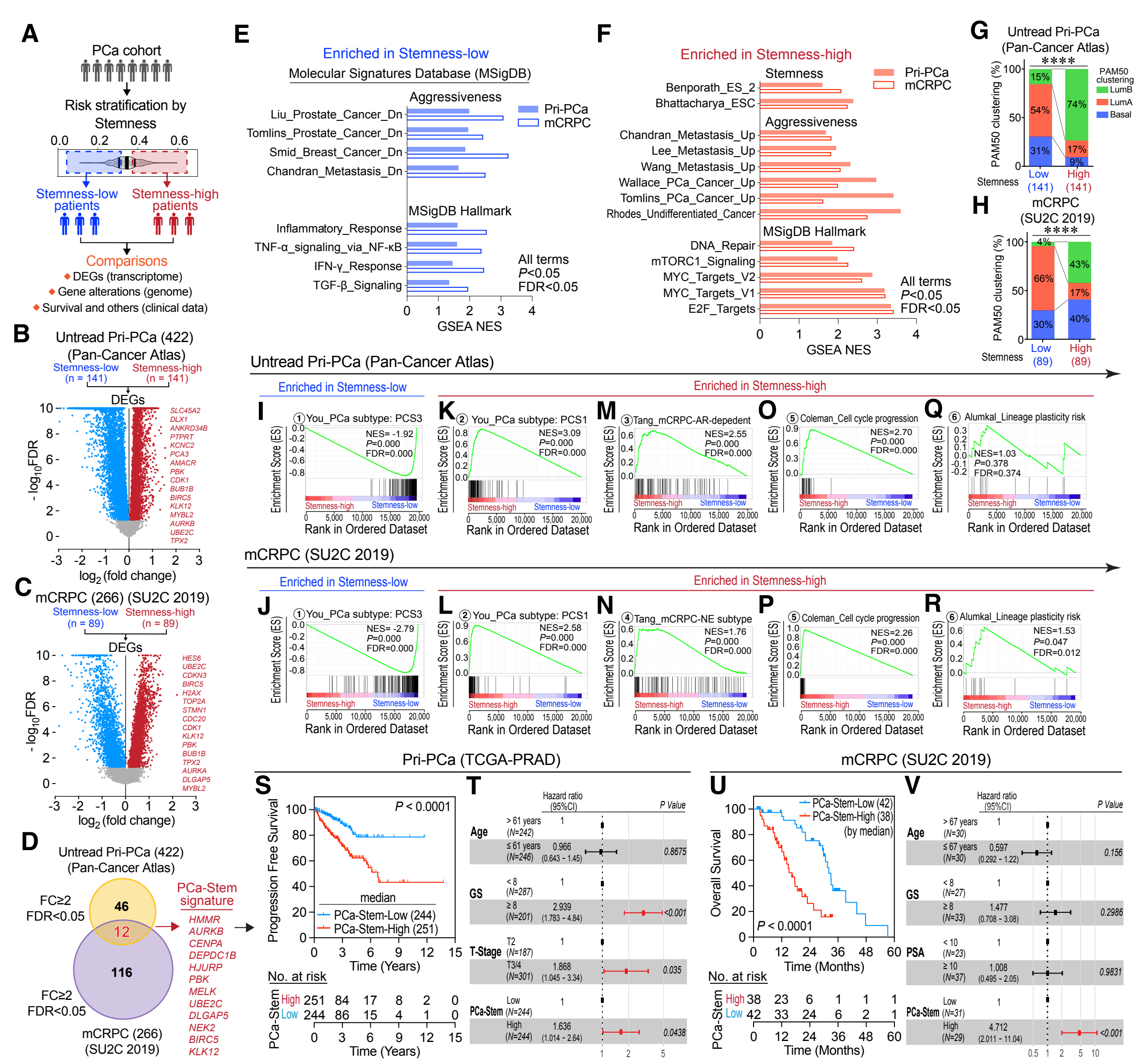
A
PCa cohort
Risk stratification by Stemness
0.0 0.2 0.4 0.6
Stemness-low patients
Stemness-high patients
Comparisons
DEGs (transcriptome)
Gene alterations (genome)
Survival and others (clinical data)
B
Untread Pri-PCa (422) (Pan-Cancer Atlas)
Stemness-low (n = 141)
Stemness-high (n = 141)
DEGs
SLC45A2 DLX1 ANKRD34B PTPRT KCNC2 PCA3 AMACR PBK CDK1 BUB1B BIRC5 KLK12 MYBL2 AURKB UBE2C TPX2
-log10FDR
log2 (fold change)
C
mCRPC (266) (SU2C 2019)
Stemness-low (n = 89)
Stemness-high (n = 89)
DEGs
HES6 UBE2C CDKN3 BIRC5 H2AX TOP2A STMN1 CDC20 CDK1 KLK12 PBK BUB1B TPX2 AURKA DLGAP5 MYBL2
-log10FDR
log2 (fold change)
D
Untread Pri-PCa (422) (Pan-Cancer Atlas)
FC≥2 FDR<0.05
46
12
116
FC≥2 FDR<0.05
mCRPC (266) (SU2C 2019)
PCa-Stem signature
HMMR AURKB CENPA DEPDC1B HJURP PBK MELK UBE2C DLGAP5 NEK2 BIRC5 KLK12
E
Enriched in Stemness-low
Molecular Signatures Database (MSigDB)
Aggressiveness
Liu_Prostate_Cancer_Dn
Tomlins_Prostate_Cancer_Dn
Smid_Breast_Cancer_Dn
Chandran_Metastasis_Dn
MSigDB Hallmark
Inflammatory_Response
TNF-α_signaling_via_NF-κB
IFN-γ_Response
TGF-β_Signaling
Pri-PCa
mCRPC
All terms P<0.05 FDR<0.05
GSEA NES
F
Enriched in Stemness-high
Stemness
Benporath_ES_2
Bhattacharya_ESC
Aggressiveness
Chandran_Metastasis_Up
Lee_Metastasis_Up
Wang_Metastasis_Up
Wallace_PCa_Cancer_Up
Tomlins_PCa_Cancer_Up
Rhodes_Undifferentiated_Cancer
MSigDB Hallmark
DNA_Repair
mTORC1_Signaling
MYC_Targets_V2
MYC_Targets_V1
E2F_Targets
Pri-PCa
mCRPC
All terms P<0.05 FDR<0.05
GSEA NES
G
Untread Pri-PCa (Pan-Cancer Atlas)
PAM50 clustering (%)
PAM50 clustering
LumB
LumA
Basal
Stemness
Low (141)
High (141)
H
mCRPC (SU2C 2019)
PAM50 clustering (%)
Stemness
Low (89)
High (89)
Untread Pri-PCa (Pan-Cancer Atlas)
Enriched in Stemness-low
Enriched in Stemness-high
I You_PCa subtype: PCS3 NES= -1.92 P=0.000 FDR=0.000
K You_PCa subtype: PCS1 NES=3.09 P=0.000 FDR=0.000
M Tang_mCRPC-AR-depedent NES=2.55 P=0.000 FDR=0.000
O Coleman_Cell cycle progression NES=2.70 P=0.000 FDR=0.000
Q Alumkal_Lineage plasticity risk NES=1.03 P=0.378 FDR=0.374
Enrichment Score (ES)
Stemness-high
Stemness-low
Rank in Ordered Dataset
mCRPC (SU2C 2019)
Enriched in Stemness-low
Enriched in Stemness-high
J You_PCa subtype: PCS3 NES= -2.79 P=0.000 FDR=0.000
L You_PCa subtype: PCS1 NES=2.58 P=0.000 FDR=0.000
N Tang_mCRPC-NE subtype NES=1.76 P=0.000 FDR=0.000
P Coleman_Cell cycle progression NES=2.26 P=0.000 FDR=0.000
R Alumkal_Lineage plasticity risk NES=1.53 P=0.047 FDR=0.012
Pri-PCa (TCGA-PRAD)
S
Progression Free Survival
P < 0.0001
median
PCa-Stem-Low (244)
PCa-Stem-High (251)
Time (Years)
No. at risk
PCa-Stem High 251 84 17 8 2 0
Low 244 86 15 4 1 0
T
Hazard ratio (95%CI)
P Value
Age > 61 years (N=242) 1
≤ 61 years (N=246) 0.966 (0.643 - 1.45) 0.8675
GS < 8 (N=287) 1
≥ 8 (N=201) 2.939 (1.783 - 4.84) <0.001
T-Stage T2 (N=187) 1
T3/4 (N=301) 1.868 (1.045 - 3.34) 0.035
PCa-Stem Low (N=244) 1
High (N=244) 1.636 (1.014 - 2.64) 0.0438
mCRPC (SU2C 2019)
U
Overall Survival
PCa-Stem-Low (42)
PCa-Stem-High (38)
(by median)
P < 0.0001
Time (Months)
No. at risk
PCa-Stem High 38 23 6 1 1 1
Low 42 33 24 6 2 1
V
Hazard ratio (95%CI)
P Value
Age > 67 years (N=30) 1
≤ 67 years (N=30) 0.597 (0.292 - 1.22) 0.156
GS < 8 (N=27) 1
≥ 8 (N=33) 1.477 (0.708 - 3.08) 0.2986
PSA < 10 (N=23) 1
≥ 10 (N=37) 1.008 (0.495 - 2.05) 0.9831
PCa-Stem Low (N=31) 1
High (N=29) 4.712 (2.011 - 11.04) <0.001

Figure 5

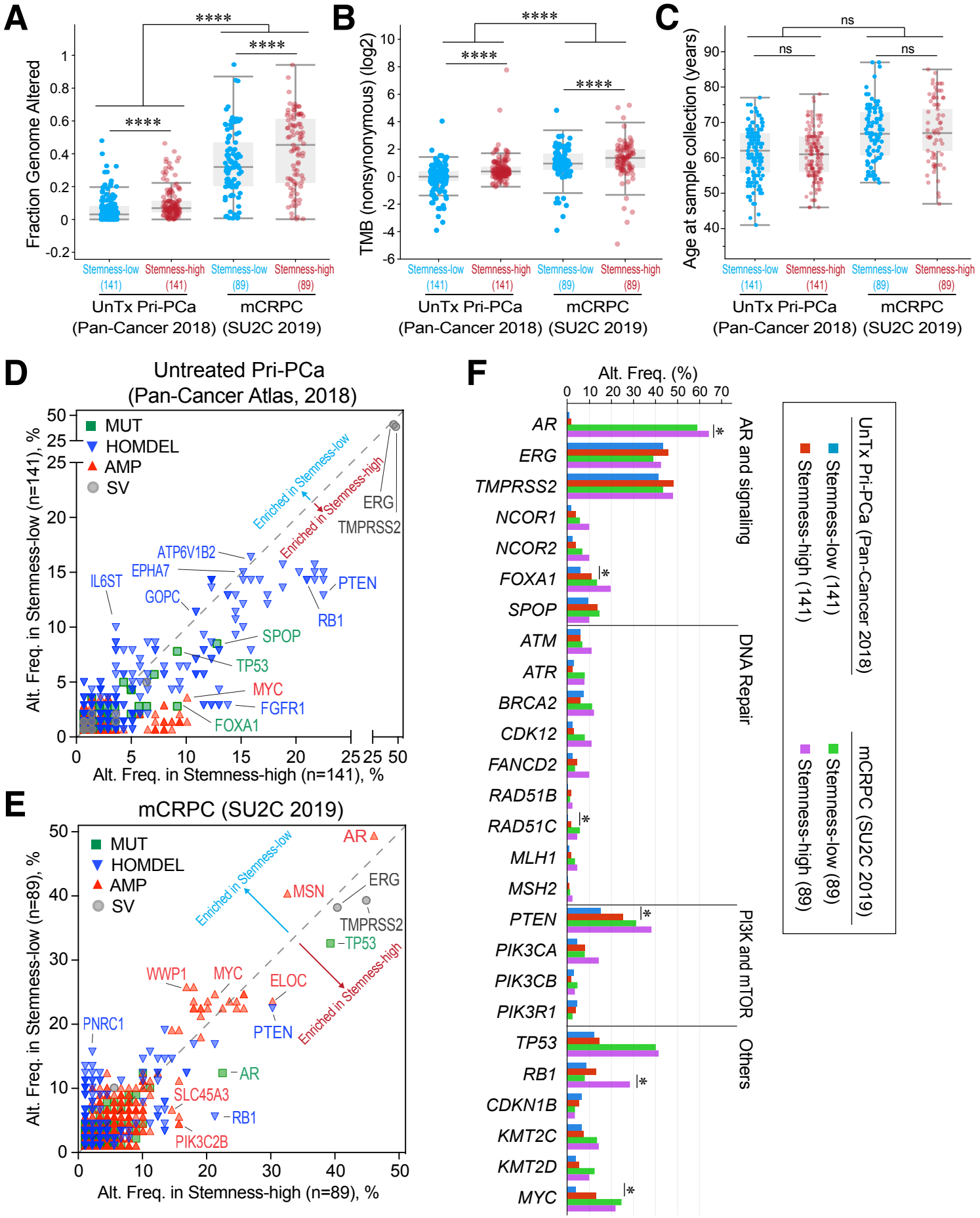
A
Fraction Genome Altered
****
****
****
Stemness-low (141)
Stemness-high (141)
Stemness-low (89)
Stemness-high (89)
UnTx Pri-PCa (Pan-Cancer 2018)
mCRPC (SU2C 2019)
B
TMB (nonsynonymous) (log2)
****
****
****
C
Age at sample collection (years)
ns
ns
ns
D
Untreated Pri-PCa (Pan-Cancer Atlas, 2018)
MUT
HOMDEL
AMP
SV
Enriched in Stemness-low
Enriched in Stemness-high
ERG
TMPRSS2
ATP6V1B2
EPHA7
IL6ST
GOPC
PTEN
RB1
SPOP
TP53
MYC
FGFR1
FOXA1
Alt. Freq. in Stemness-low (n=141), %
Alt. Freq. in Stemness-high (n=141), %
E
mCRPC (SU2C 2019)
MUT
HOMDEL
AMP
SV
Enriched in Stemness-low
Enriched in Stemness-high
AR
MSN
ERG
TMPRSS2
TP53
WWP1
MYC
ELOC
PNRC1
PTEN
AR
SLC45A3
RB1
PIK3C2B
Alt. Freq. in Stemness-low (n=89), %
Alt. Freq. in Stemness-high (n=89), %
F
Alt. Freq. (%)
AR
ERG
TMPRSS2
NCOR1
NCOR2
FOXA1
SPOP
ATM
ATR
BRCA2
CDK12
FANCD2
RAD51B
RAD51C
MLH1
MSH2
PTEN
PIK3CA
PIK3CB
PIK3R1
TP53
RB1
CDKN1B
KMT2C
KMT2D
MYC
AR and signaling
DNA Repair
PI3K and mTOR
Others
UnTx Pri-PCa (Pan-Cancer 2018)
Stemness-low (141)
Stemness-high (141)
mCRPC (SU2C 2019)
Stemness-low (89)
Stemness-high (89)

Figure 6

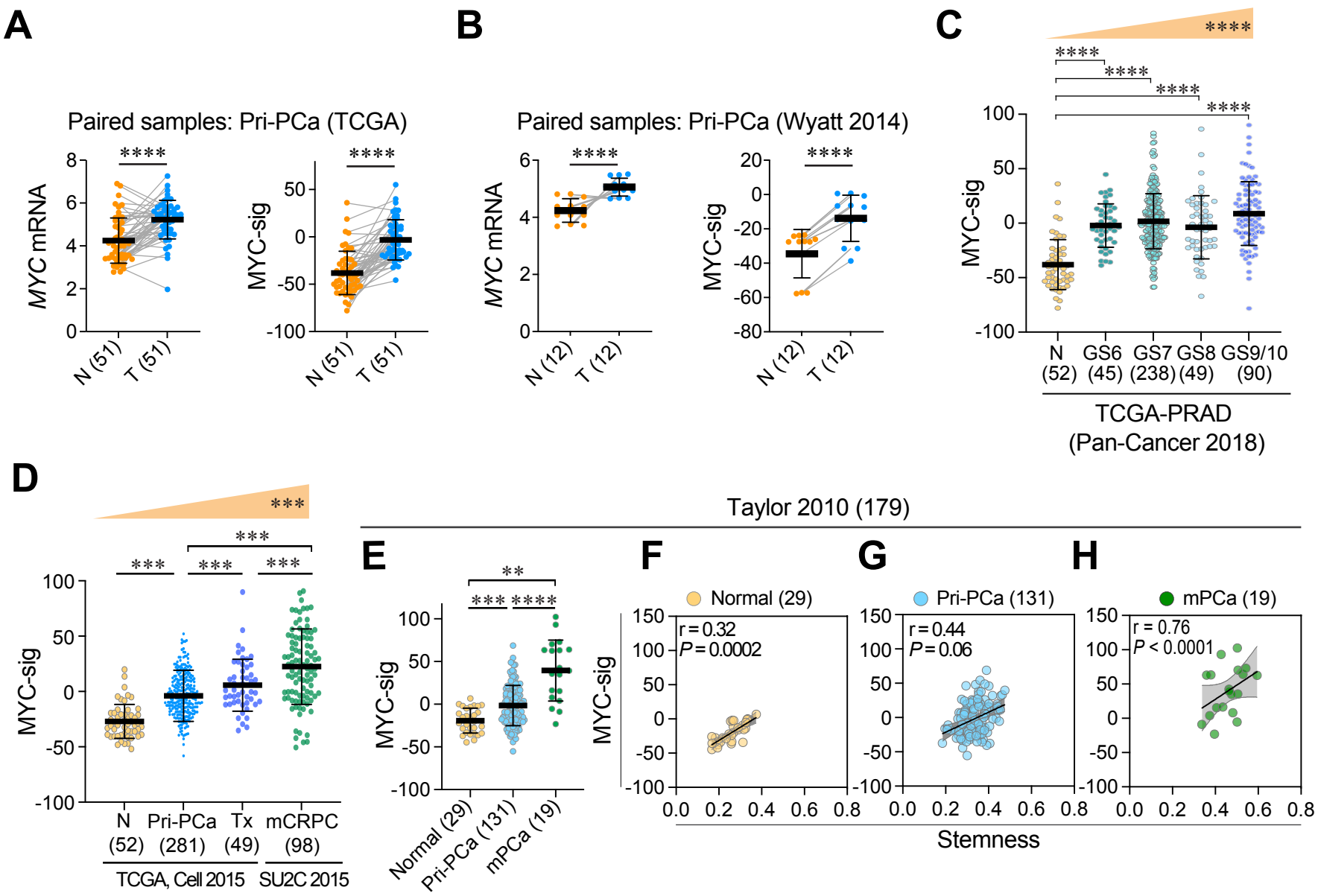
A
Paired samples: Pri-PCa (TCGA)
MYC mRNA
MYC-sig
****
N (51)
T (51)
B
Paired samples: Pri-PCa (Wyatt 2014)
MYC mRNA
MYC-sig
****
N (12)
T (12)
C
MYC-sig
****
N (52)
GS6 (45)
GS7 (238)
GS8 (49)
GS9/10 (90)
TCGA-PRAD
(Pan-Cancer 2018)
D
MYC-sig
***
N (52)
Pri-PCa (281)
Tx (49)
mCRPC (98)
TCGA, Cell 2015
SU2C 2015
Taylor 2010 (179)
E
MYC-sig
**
***
****
Normal (29)
Pri-PCa (131)
mPCa (19)
F
Normal (29)
r = 0.32
P = 0.0002
G
Pri-PCa (131)
r = 0.44
P = 0.06
H
mPCa (19)
r = 0.76
P < 0.0001
MYC-sig
Stemness

Figure 7

Supplementary Information Content

Increasing Stemness Drives Prostate Cancer Progression, Plasticity, Therapy Resistance and Poor Patient Survival

Liu X, Cortes E, et al.

Supplementary Table S1. Summary of datasets used in this study
Supplementary Table S2. Summary of gene signatures used in this study
Supplementary Table S3. DEGs identified in Stemness-high versus Stemness-low subgroups in the Pri-PCa (TCGAPRAD) cohort and in the mCRPC (SU2C 2019) cohort (*six sheets)
Supplementary Table S4. Summary of statistical significance of differences using Tukey's multiple comparisons test (*three sheets)
Supplementary Table S5. Summary of gene signatures and gene sets used in Gene Set Enrichment Analysis

Related to Fig. 1
Supplementary Fig. S1. Schematic illustration of bioinformatic datasets and signature score pipelines used for comparisons across the spectrum of PCa evolution.
Supplementary Fig. S2. Transcriptome-based signature scores for canonical (pro-differentiation) AR signaling activity (AR-A).
Supplementary Fig. S3. Prostate luminal cell compartment harbors higher AR-A but lower Stemness as compared to prostate basal cell compartment.

Supplementary Fig. S4. nADT decreases both AR-A and Stemness.

Related to Fig. 3
Supplementary Fig. S5. Increased Stemness represents a 'universal' feature of PCa progression and aggressiveness.

Related to Fig. 4
Supplementary Fig. S6. High Stemness correlates with poor patient survival.

Related to Fig. 5
Supplementary Fig. S7. PCa-Stem signature and gene expression correlate with PCa progression.

Related to Fig. 6
Supplementary Fig. S8. Unique genomic features of Stemness-high PCa.

Related to Fig. 7
Supplementary Fig. S9. Lack of effect of nADT on MYC activity.

Supplementary Fig. S10. Schematic summary of PCa progression and aggressiveness accompanied by gain of oncogenic Stemness and loss of prostatic epithelium differentiation defined by canonical AR signaling.

Supplementary Figure S1

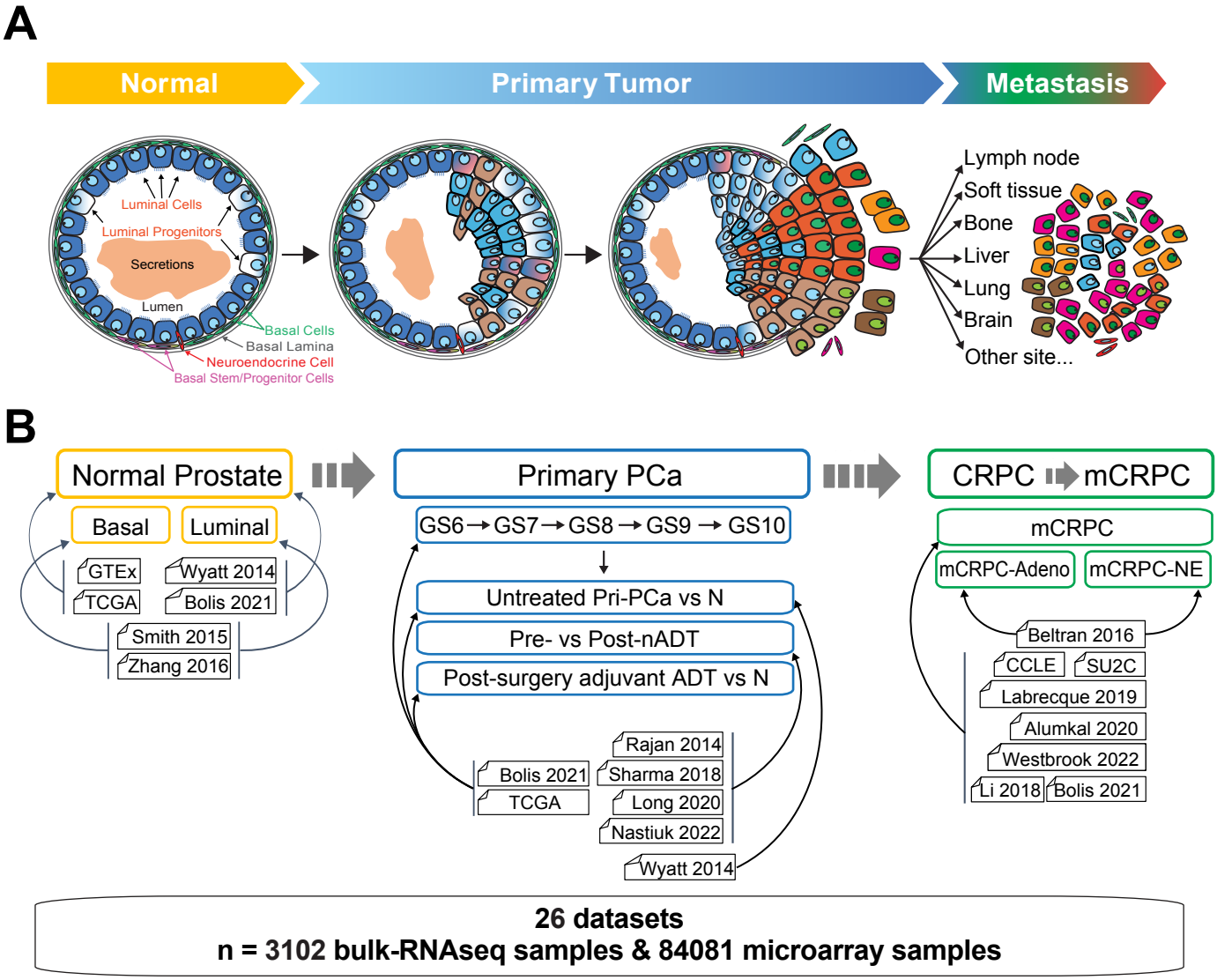

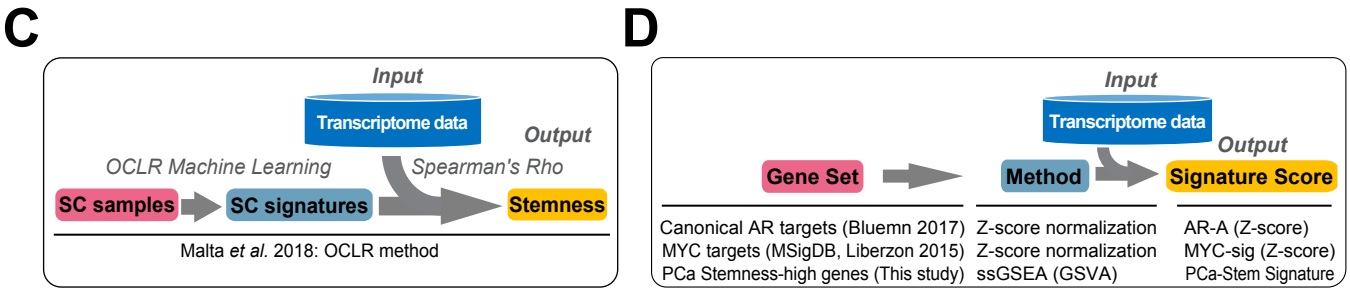

Supplementary Figure S1. Schematic illustration of bioinformatic datasets and signature score pipelines used for comparisons across the spectrum of PCa evolution.

(A-B) Schematic illustrating the spectrum of PCa development, therapy resistance, and metastatic progression (A), and related datasets used for comparisons in different contexts (B). Panel A illustrates the PCa progression continuum from Normal Prostate (Normal) through Primary PCa (Pri-PCa), to Castration-Resistant PCa (CRPC) and Metastatic CRPC (mCRPC), with each stage marked by specific changes in cellular composition and architectural organization. Panel B details the datasets utilized for comparative analyses across these stages, with arrows indicating the relationship of each dataset to specific PCa stages. In total, 26 datasets were used in the current analysis, including 3102 bulk-RNAseq samples and 84081microarray samples. See Supplementary Table S1 for dataset details. (A is adapted from ref. 7).

Detailed Description of PCa Stages:

- Normal Prostate: Depicted as a glandular organ with a pseudostratified two-layer epithelium consisting of basal and luminal cells, interspersed with rare neuroendocrine cells. Luminal cells express cytokeratins CK8 and CK18, androgen receptor (AR), and prostate-specific antigen (PSA), and represent the primary secretory cells. Also depicted are rare luminal progenitor cells within the luminal cell layer, which represent less than 2 % of the luminal cell population and are characterized by the co-expression of CK5 and CK8 and a low level of CD38 (reviewed in ref. 8). Basal cells express CK5 and CK14, interfacing with the stroma through the basal lamina. The basal cell compartment harbors stem/progenitor cells capable of bidirectional differentiation (ref. 8). Also see an enlarged depiction of a normal human prostatic gland in Supplementary Fig. S3A.
- Localized Pri-PCa: Progresses from well-differentiated structures (low Gleason score) to poorly differentiated configurations (high Gleason score), indicating a shift towards a more stem-like state with loss of glandular architecture. This transition involves a reduction in basal cells and an expansion of progenitor-like cells, with the combined Gleason score (GS) reflecting the architectural patterns of cancerous glands. Gleason pattern 1 represents the most well-differentiated glandular structures and Gleason pattern 5 consists of the most poorly differentiated cells lacking glandular structures. Given that PCa is often multifocal, the combined GS is the sum of the two most prevalent patterns, with GS ≤ 7 representing low-grade PCa and GS ≥ 8 representing high-grade PCa. Illustrated here are two representative tumor glands with a decrease/loss in basal cells and expansion of luminal progenitor-like cells.
- Metastatic CRPC: Features increased cellular heterogeneity and the presence of cells with stem-like and neuroendocrine-like characteristics, which drive therapy resistance and disease progression.

(C-D) Schematic presentation of transcriptome-based stemness quantification method mRNAsi (C, ref. 6), and transcriptome-based signature scores for canonical AR signaling activity levels, MYC signaling activity levels and PCa-Stem signature (D). See Supplementary Table S2 for gene signature information.

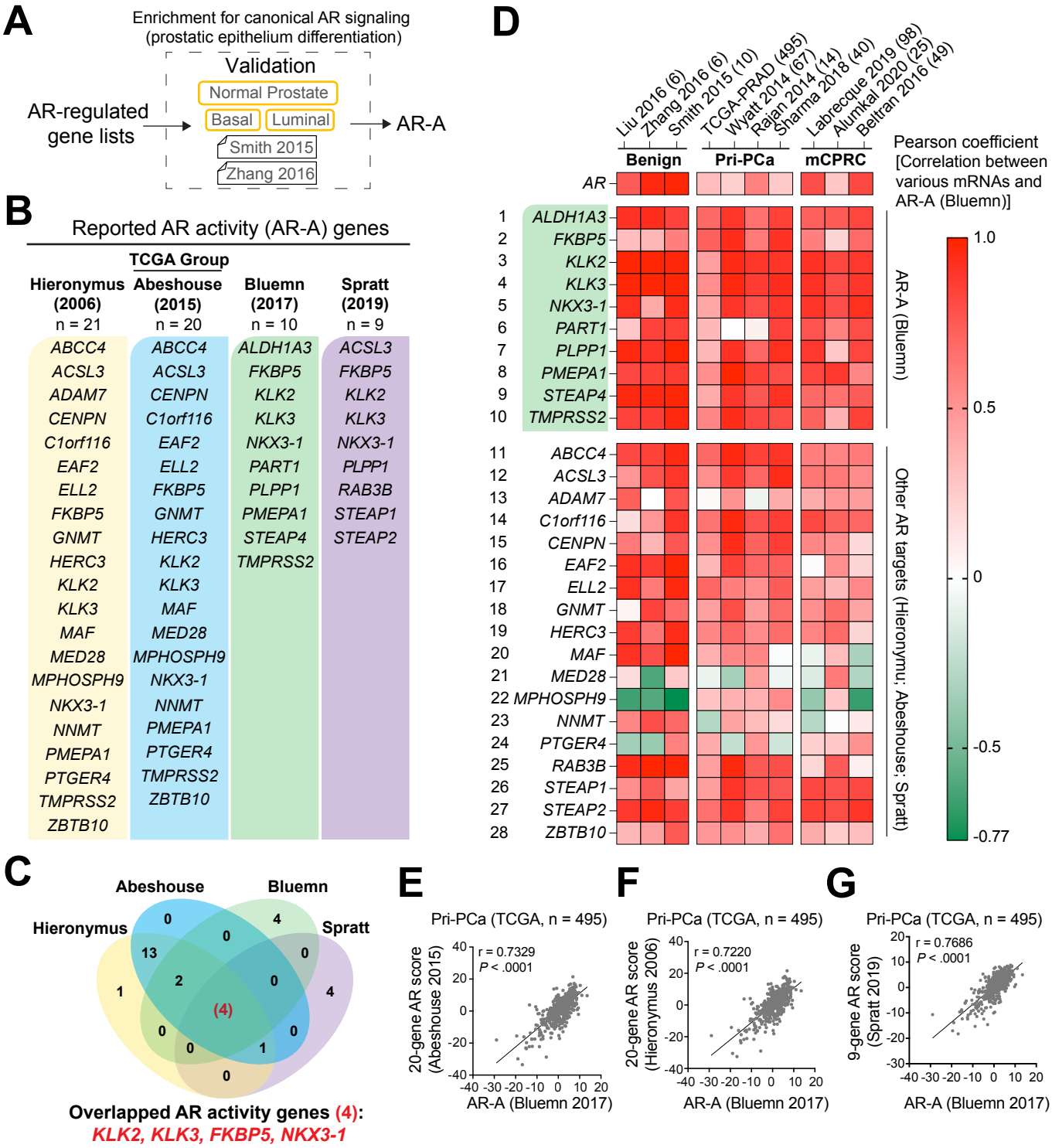

Supplementary Figure S2. Transcriptome-based signature scores for canonical (pro-differentiation) AR-A.

(A) Workflow for validating canonical AR signaling activity (AR-A) signatures from different AR-regulated gene lists.

(B-C) Comparison of AR downstream signaling targets from four studies. The 4 genes commonly shared in all four AR-A signatures are highlighted (C). Genes were listed using updated HGNC symbols (the HUGO gene nomenclature from the Human Genome Organization). Note that in the original publications, some AR-A genes were denoted by their (gene/protein) aliases, as exemplified by *CENPN (BM039), C1orf116 (SARG), KLK3 (PSA), PLPP1 (PPAP2A), and PMEPA1 (TMEPAI)*.

(D) AR-A signature score highly correlates with mRNA expression levels of canonical AR signaling targets in various PCa related cohorts. See Supplementary Table S1 for dataset details.

(E-G) Strong positive linear relationships between the Bluemn AR-A and the other three AR-A signatures (Hieronymus 2006; Abeshouse 2015, Spratt 2019) using primary PCa cohort (TCGA-PRAD). r indicates Pearson correlation coefficient.

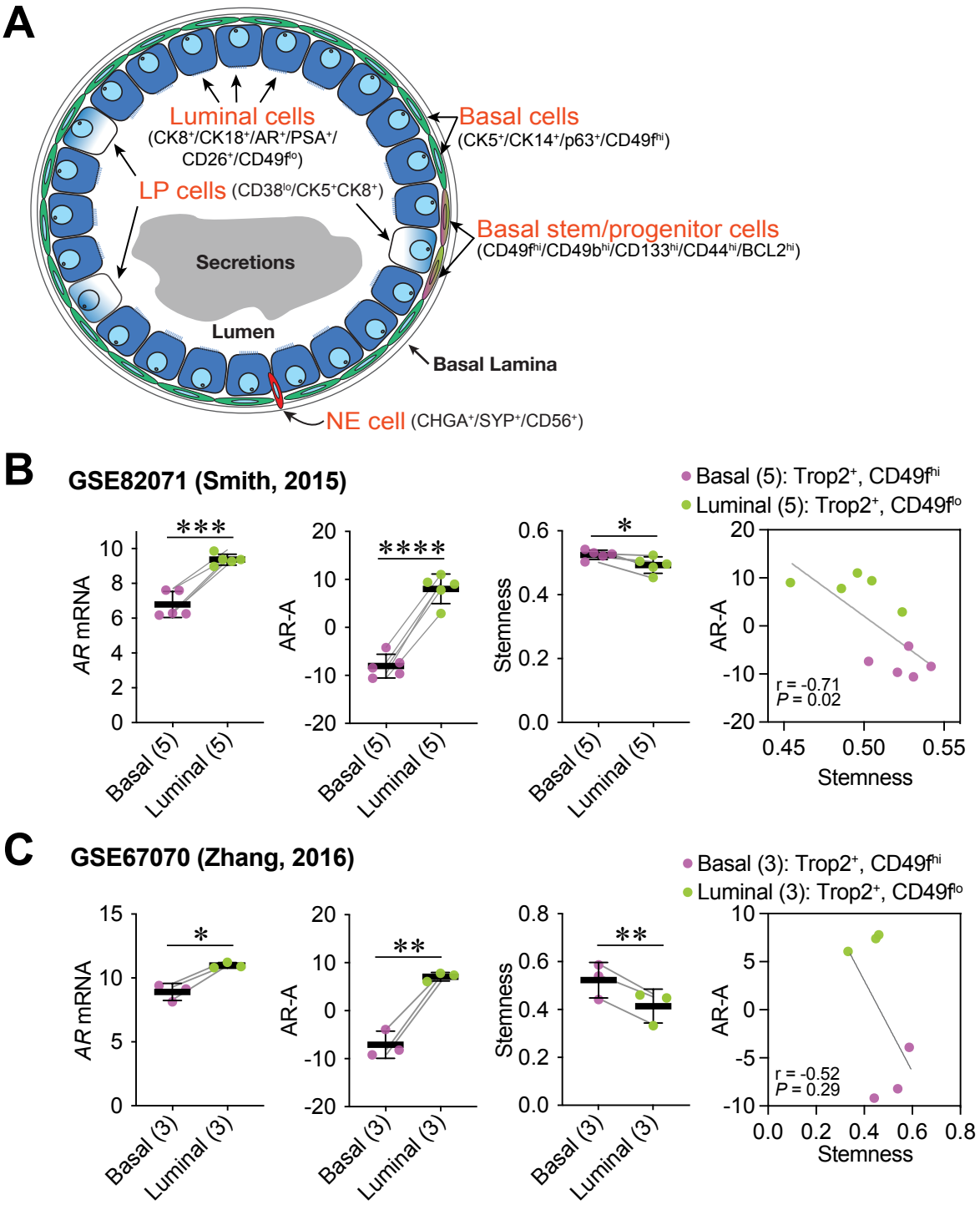

Supplementary Figure S3. Prostate luminal cell compartment harbors higher AR-A but lower Stemness as compared to prostate basal cell compartment.

(A) Depiction of the major cell types in human prostatic glands. Both basal and luminal cell compartments harbor differentiated as well as less mature stem/progenitor cells. LP, luminal progenitor; NE, neuroendocrine. Cellular markers are highlighted for different cell types. Adapted from ref. 8.

(B-C) Prostate luminal cells possess higher AR-A but lower Stemness as compared to prostate basal cells, and Stemness inversely correlates with AR-A in the context of prostatic basal and luminal cells. Results are shown as mean ± SD. The pairs are linked with a grey line. Significance was calculated by two-tailed paired Student's *t*-test (*, $P < 0.05$; **, $P < 0.01$; ***, $P < 0.001$; ****, $P < 0.0001$). Pearson correlation coefficients (Pearson's r) were used to calculate the correlations between Stemness and AR-A.

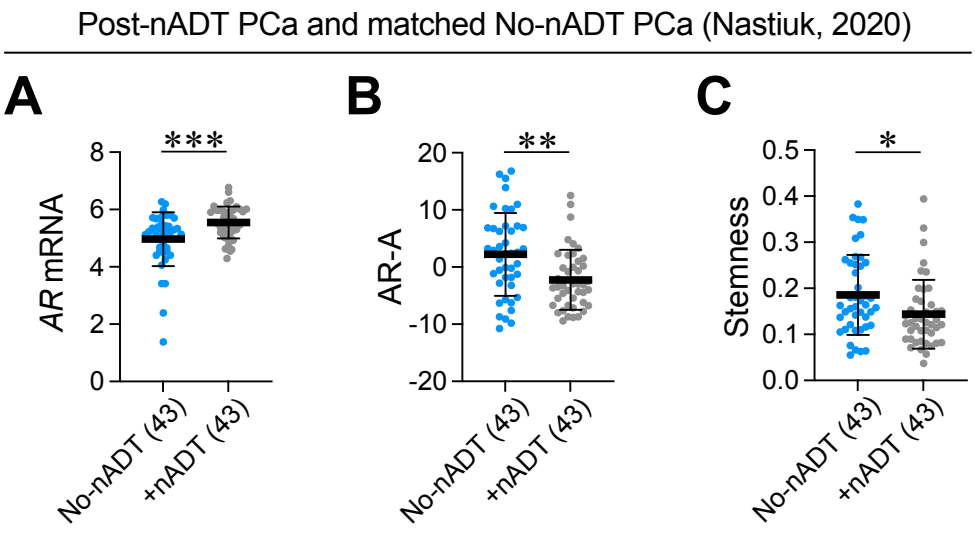

Supplementary Figure S4. nADT decreases both AR-A and Stemness.

Matched comparison of *AR* mRNA levels (A), AR-A (B), and Stemness (C) showing significant decrease of both AR-A and Stemness in neo-adjuvant ADT (+nADT) group as compared to the samples without nADT (No-nADT) from stage-, tumor grade-, age-matched PCa individuals (RPCI Nastiuk cohort). Sample sizes are indicated. See Supplementary Table S1 for cohort and RNAseq data information. Within the plots, results are shown as the mean ± SD. Significance was calculated by two-tailed unpaired Student's *t*-test (*, $P < 0.05$; **, $P < 0.01$; ***, $P < 0.001$).

Supplementary Figure S5

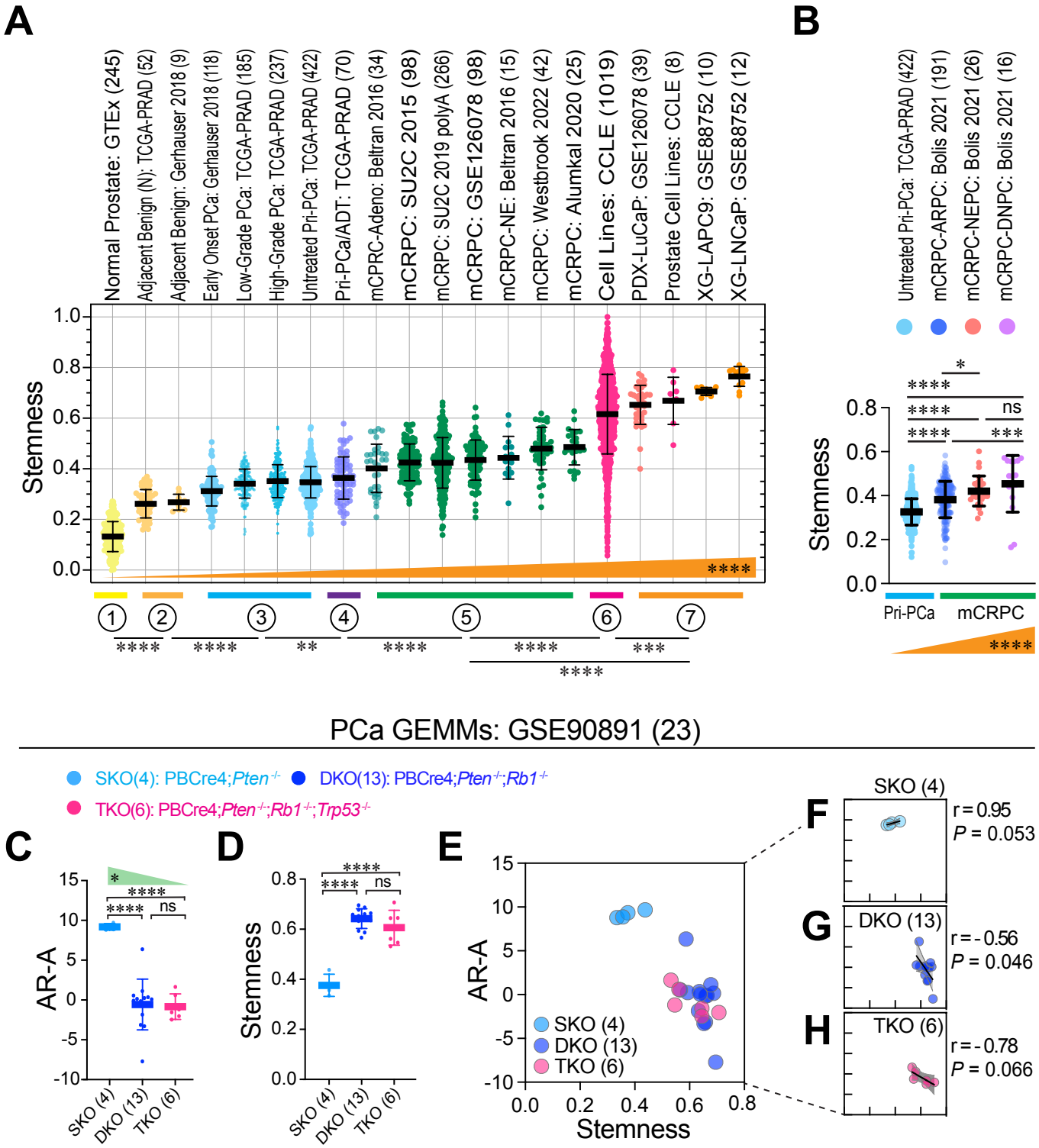

Supplementary Figure S5. **Increased Stemness represents a 'universal' feature of PCa progression and aggressiveness.**

(A) Increasing Stemness accompanies PCa progression and aggressiveness. Stemness scores were shown in various PCa cohorts representing the PCa evolutionary spectrum (from top to bottom): GTEx normal prostate → TCGA tumor-adjacent benign prostate tissue → Treatment-naïve Pri-PCa → aggressive Pri-PCa treated with adjuvant hormone therapy Pri-PCa/ADT → Treatment-failed CRPC → mCRPC → Long-term PCa models including PDX, xenografts (XG) and cell lines. Sample sizes (n) are indicated in the last parentheses. See Supplementary Table S1 for dataset details and Supplementary Table S4 for the statistical significance between different groups.

(B) Progressive increase in Stemness from primary PCa to advanced mCRPC subtypes. This violin plot displays increasing Stemness scores across four PCa groups, defined by treatment status and pathway activity: treatment-naïve Pri-PCa from TCGA, and three subtypes of mCRPC categorized by AR and NE pathway activities - AR pathway-active (ARPC), neuroendocrine (NEPC), and double-negative (DNPC). These three subtypes were delineated based on established signatures (Bluemn *et al.*, 2017, ref. 14; Labrecque *et al.,* 2019, ref. 33). Displayed from left to right are: Untreated Pri-PCa (n = 422), mCRPC-ARPC (191), mCRPC-NEPC (26), and mCRPC-DNPC (16). Pri-PCa samples originated from TCGA, while mCRPC samples were derived from studies by Sharp *et al.* (2019, ref. 67, GSE118435), Labrecque *et al.* (2019, ref. 33, GSE126078), Nyquist *et al.* (2020, ref. 68, GSE147250), Lim *et al.* (2021, ref. 70, GSE171729), and Beltran *et al.* (2016, ref. 28, PRJNA282856; dbGaP: phs000909). Normalized RNAseq data were sourced from the Bolis 2021 integrated cohort (ref. 27). For dataset details, see Supplementary Table S1.

(C-H) PCa progression in GEMMs is characterized by decreasing AR-A and increasing Stemness in aggressive DKO and TKO tumors. The Stemness and AR-A were analyzed in distinct genetically engineering mouse models (GEMMs) of PCa due to individual or combined deletion of 3 tumor suppressor genes, *Pten*, *Rb1* and *Trp53* (Ku *et al*., 2017, ref. 37). Briefly, *Pten*$^{-/-}$ single knockout (SKO) prostate tumors develop around 9 weeks, and mice rarely develop metastasis with a median lifespan of 48 weeks. In contrast, the *Pten*$^{-/-}$;*Rb1*$^{-/-}$ double knockout (DKO) mice develop highly metastatic PCa that shortens median survival to ~38 weeks. DKO tumors are initially castration-sensitive but eventually become castration-resistant and, notably, castration-resistant DKO tumors turn into an AR$^{-/lo}$ phenotype. When *Trp53* is further deleted in DKO background, the triple KO (TKO; *Pten*$^{-/-}$;*Rb1*$^{-/-}$;*Trp53*$^{-/-}$) tumors are exclusively AR^{-} NEPC and castration-resistant *de novo* with high metastatic rate and lifespan of ~16 weeks. AR-A was dramatically reduced (C) but Stemness was significantly increased (D) in the aggressive DKO and TKO PCa compared to indolent SKO prostate tumors. E-H, Scatter plots illustrating the correlations between AR-A and Stemness in combined cases in PCa GEMMs (E), SKO (F, Pearson's r=0.95, P = 0.053), DKO (G, Pearson's r= –0.56, P = 0.053), and TKO (H, Pearson's r= –0.78, P = 0.066).

All data in dot plots and violin plots are shown as mean ± SD. Statistical significance was determined using one-way analysis of variance (ANOVA) followed by Tukey's multiple-comparison test. Jonckheere-Terpstra's trend (J-T) test was used to calculate the statistical significance of the trend across different groups. Pearson correlation coefficients (Pearson's r) were used to calculate the correlations between the Stemness and AR-A. Note: ns, not significant; *, P < 0.05; **, P < 0.01; ***, P < 0.001; ****, P < 0.0001.

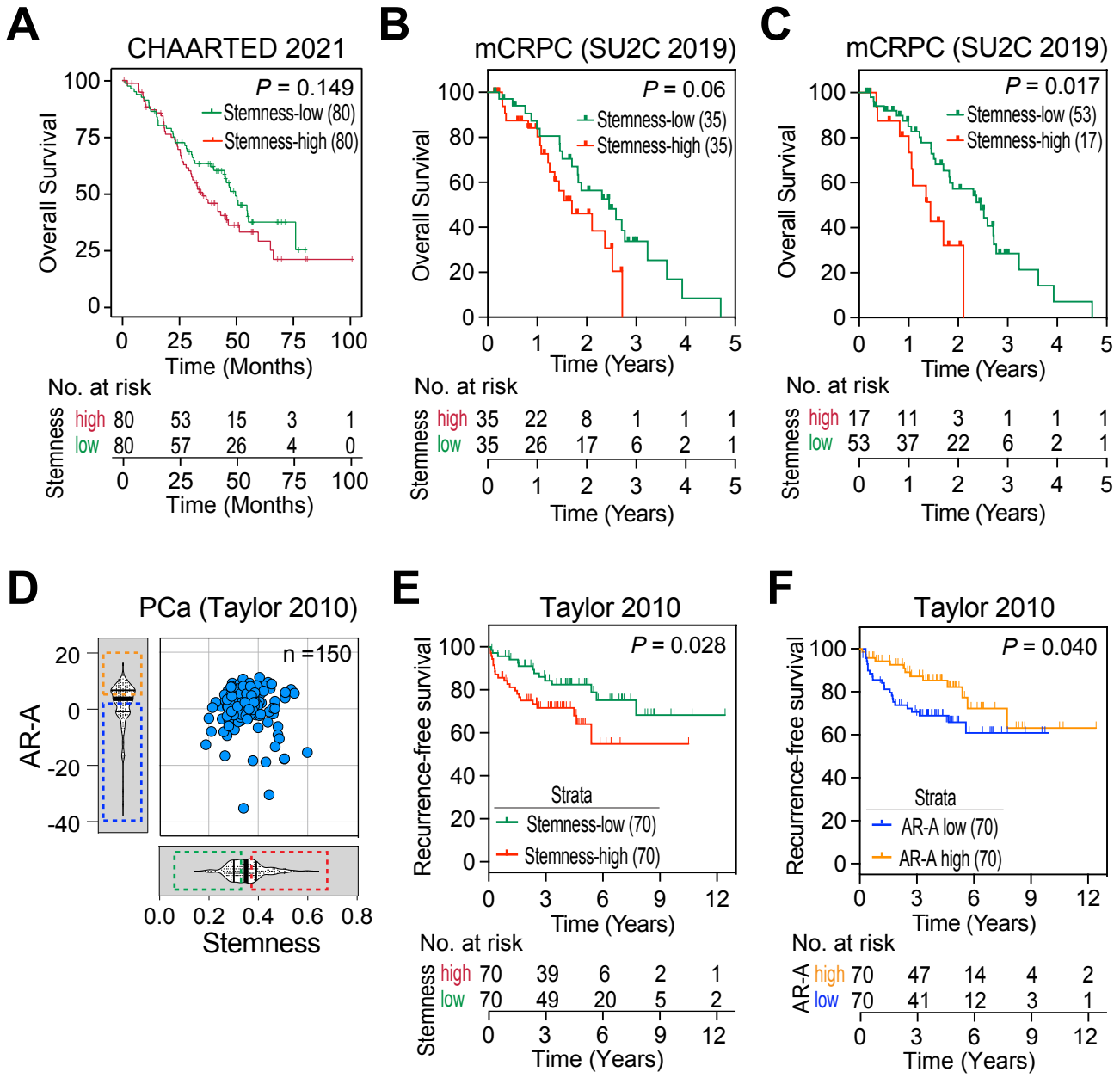

Supplementary Figure S6. High Stemness correlates with poor patient survival.

(A-C) High Stemness correlates with poorer overall survival in CHAARTED 2021 cohort (A) or SU2C mCRPC cohort (B-C). The CHAARTED 2021 cohort was divided into Stemness-high (n = 80) and Stemness-low (n = 80) using Stemness median split (A). The SU2C 2019 mCRPC cohort was divided into Stemness-high and Stemness-low using Stemness median split (B) or the analysis was done by comparing the 25% of highest Stemness samples with the 75% of lowest Stemness samples (C). *P*-value was determined using the Log-Rank test.

(D-F) High Stemness and low AR-A correlate with worse recurrence-free survival in PCa patients in the Taylor 2010 PCa cohort. Stemness (E) or AR-A (F) was used to fractionate Taylor cohort for Kaplan-Meier analysis. The Taylor patient cohort was divided into Stemness-high (n = 70) and Stemness-low (n = 70) using Stemness median split (E) or AR-A high (n = 70) and AR-A low (n =70) using AR-A median split (F) followed by the Kaplan-Meier analyses. Note: there are 150 PCa samples with transcriptome data in the Taylor cohort but only 140 PCa samples with survival data. *P*-value was determined using the Log-Rank test.

Supplementary Figure S7

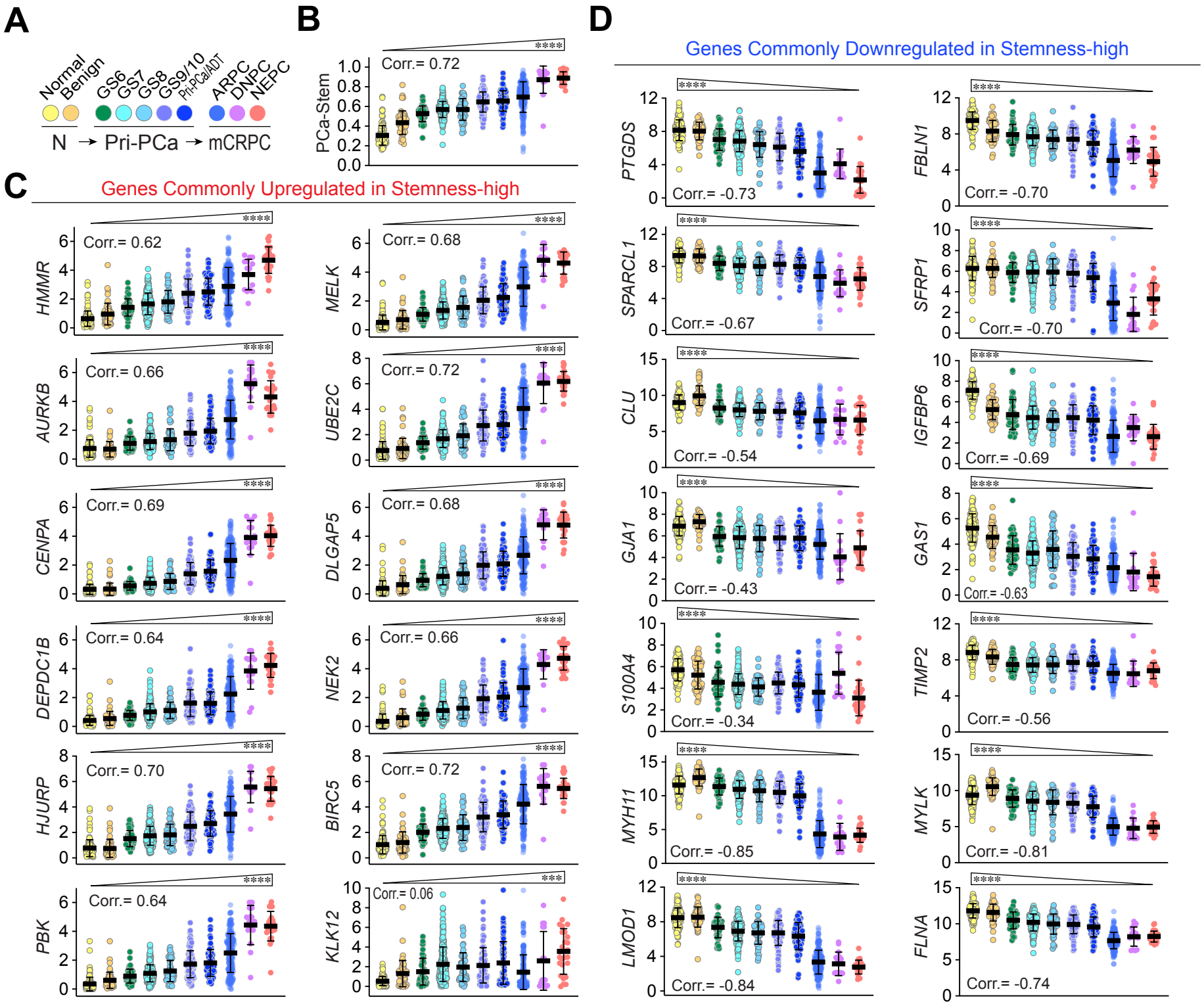

Supplementary Figure S7. PCa-Stem signature and gene expression correlate with PCa progression.

(A) Schematic of PCa continuum, from normal prostate (N) through various stages of primary PCa (Pri-PCa) to treatment-failed mCRPC. Sample groups include:

- Two subgroups in N (Normal/Benign), including GTEx normal prostate (n=116) and TCGA tumor-adjacent benign prostate tissue (n=52).
- Five subgroups in Pri-PCa, including GS6 (n=45), GS7 (n=238), GS8 (n=49), combined GS9 and GS10 (GS9/10; n=90), and aggressive Pri-PCa treated with post-surgery adjuvant hormone therapy (Pri-PCa/ADT; n=70).
- Three subtypes of mCRPC, including AR-active PCa (ARPC; n=191), double-negative AR-null/neuroendocrine-null PCa (DNPC; n=16), and neuroendocrine PCa (NEPC; n=26).

*Note that the color-coded entities of normal/benign prostate and progressive PCa stages in panel A also represent the legend for all dot plots in panels B-D.

(B) Dot plot showing the increasing 12-gene PCa-Stem signature scores positively correlate with the PCa progression described in (A).

(C) Dot plots showing that the mRNA levels of 11 of the 12 PCa-Stem signature genes (i.e., *HMMR, AURKB, CENPA, DEPDC1B, HJURP, PBK, MELK, UBE2C, DLGAP5, NEK2,* and *BIRC5)* except *KLK12* (see Figure 5D; Supplementary Table S3) exhibited stage-related increases and positively correlated with PCa progression.

(D) Dot plots showing that the mRNA levels for 14 genes commonly downregulated in Stemness-high groups (i.e., *PTGDS, SPARCL1, CLU, GJA1, S100A4, MYH11, LMOD1, FBLN1, SFRP1, IGFBP6, GAS1, TIMP2, MYLK, and FLNA; see* Supplementary Table S3) all individually displayed stage-related downregulation and negatively correlated with PCa progression.

For all dot plots, the Pearson's correlation coefficients (Corr.) are shown for the relationships between PCa progression scores (derived from trajectory inference analysis in the PCa transcriptome atlas; Bolis 2021; ref.27) and either PCa-Stem signature scores (B) or individual gene expression levels (C, D).

Dot plots display the mean ± SD. Trends across groups were assessed using the Jonckheere-Terpstra (J-T) trend test (wedges above). ***, $P < 0.001$; ****, $P < 0.0001$; ns, not significant.

Data Source: Normalized RNA-seq data across the stages (shown in the legend in A) were obtained from the integrated transcriptomic framework of PCa (Bolis 2021; ref.27).

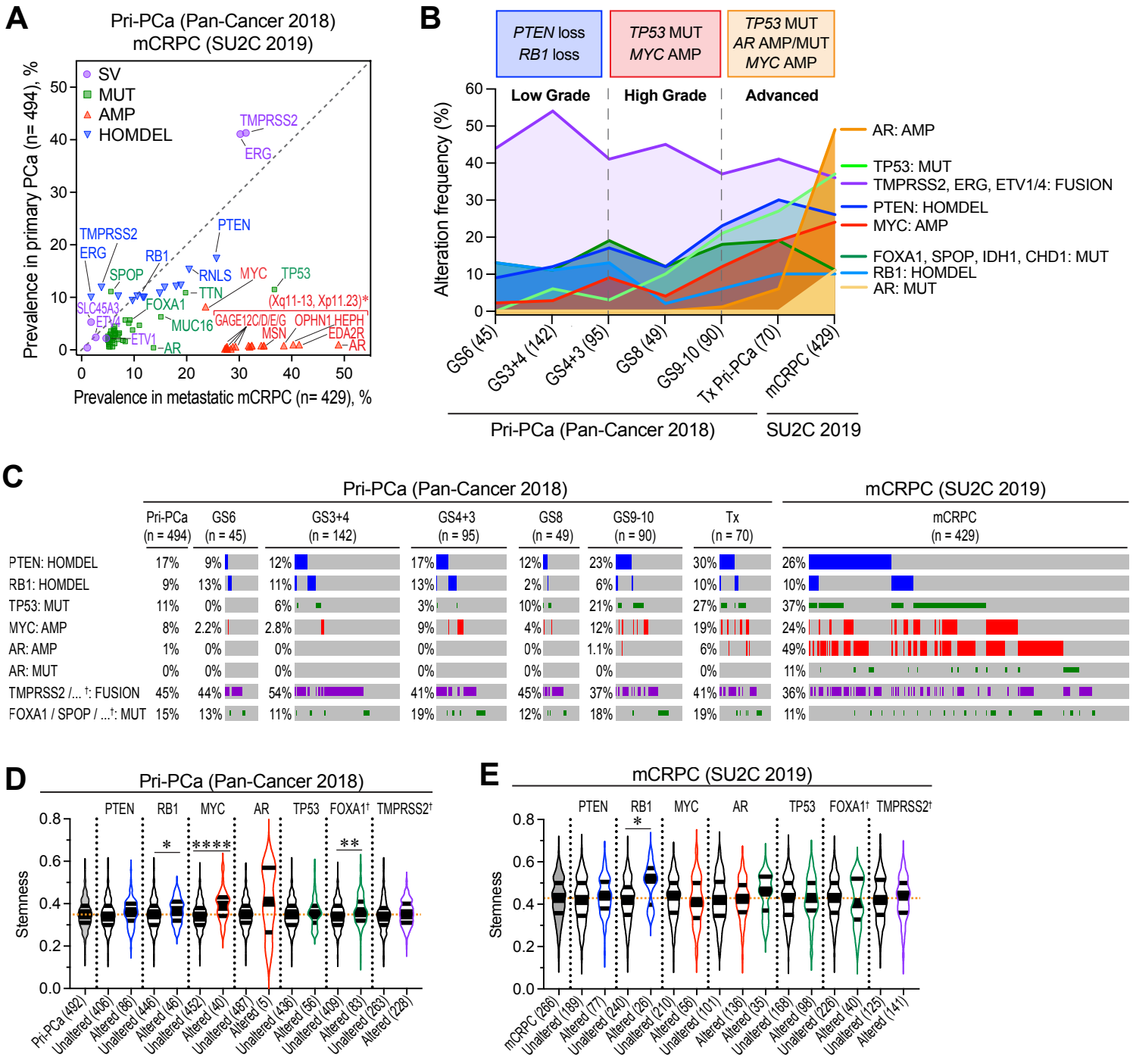

Supplementary Figure S8. Unique genomic features of Stemness-high PCa.

(A) Scatterplot of observed frequencies of genomic alterations in cancer genes reported in Pri-PCa (TCGA) versus mCRPC (SU2C) with data retrieved from cBioPortal. SV (purple), structural variants/fusions; MUT (green), mutation; AMP (red), amplification in DNA copy numbers (i.e., copy number alterations (CNA) ≥ 2); HOMDEL (blue), homozygous deletion or deep deletion.

(B) Genomic alteration frequency plot showing that (early-stage) low-grade PCa have prevalent *PTEN* and *RB1* loss and high-grade PCa have frequent *TP53* MUT and *MYC* AMP whereas advanced PCa have prevalent *TP53* MUT, *MYC* AMP and *AR* AMP/MUT.

(C) cBioPortal Oncoprint showing the frequencies of major genetic alteration events along the PCa progression continuum.

(D-E) Association of major genomic alterations in PCa with Stemness. Grey, no alterations; Blue, HOMDEL; Green, MUT; Red, AMP; Purple, Fusion. TMPRSS2 /...†: FUSION (in C) or TMPRSS2† (in D-E) stands for combined fusion events in *TMPRSS2*, *ERG*, *ETV1* and *ETV4*; FOXA1 / SPOP /...†: MUT (in C) or FOXA1† (in D-E) represent combined mutation events in *FOXA1*, *SPOP*, *IDH1* and *CHD1*. Note that data presented represent the major mutation subtypes in Pri-PCa (TCGA PRAD cohort) reported in Cancer Genome Atlas Research Network 2015 (Abeshouse *et al.*, 2015, ref. 18) and alterations (mutations, structural variants and copy number) of unknown significance were excluded. Within the violin plots, the center lines represent median values, and box edges are 75th and 25th percentiles. Significance was calculated by Mann-Whitney test (*, $P < 0.05$; **, $P < 0.01$; ****, $P < 0.0001$).

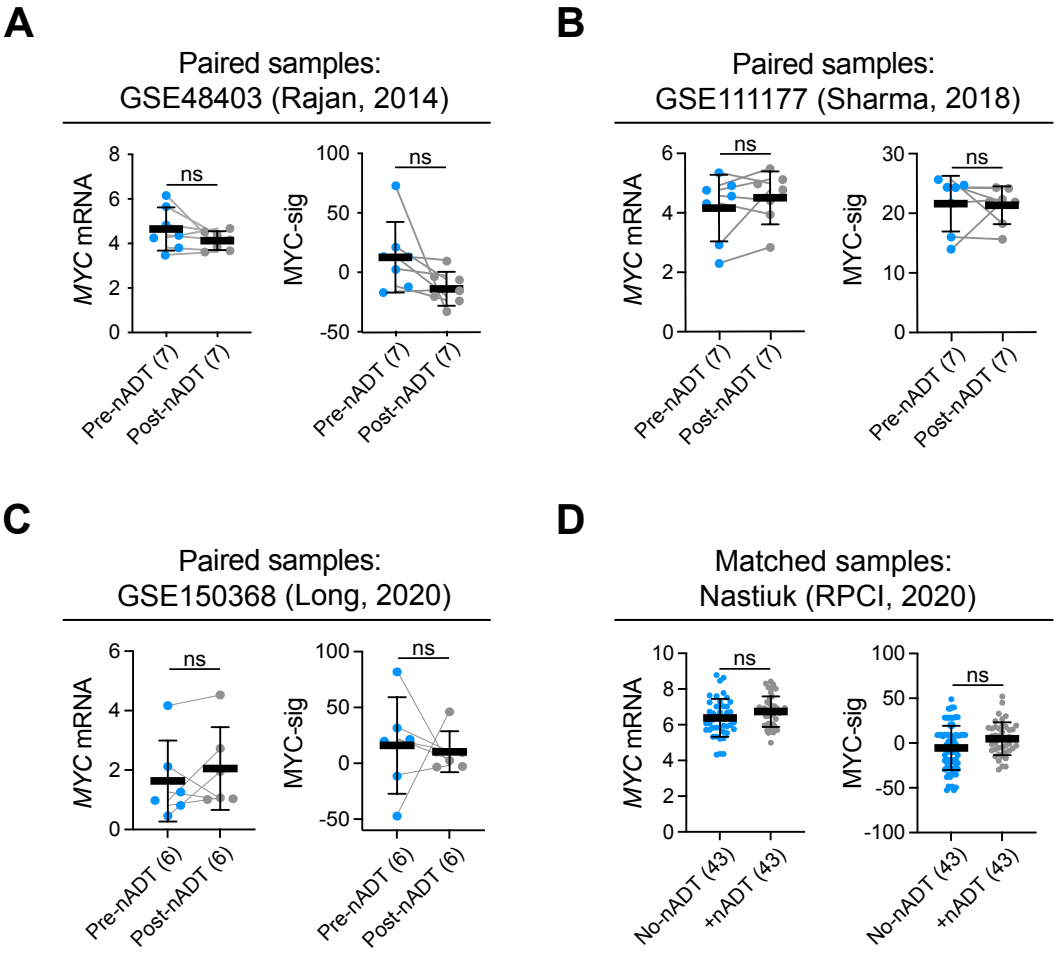

Supplementary Figure S9. Lack of effect of nADT on MYC activity.

Matched comparisons showing no significant differences in both *MYC* mRNA and MYC-sig after neo-adjuvant ADT (Post-nADT) as compared to the matched samples before nADT (Pre-nADT) from the same individuals in **A**, Rajan 2014 cohort; **B**, Sharma 2018 cohort; and **C**, Long 2020 cohort or in **D**, the RPCI Chatta/Nastiuk cohort (unpublished) comprising PCa samples from patients who received nADT (+nADT) and the patients who did not receive ADT (no-ADT) but otherwise matched (with the +nADT patients) for ages and tumor stage and grade.
Sample sizes are indicated in parentheses. Within the plots, results are shown as the mean ± SD. The pairs are linked with a grey line. Significance was calculated by two-tailed paired (A-C) or unpaired (D) Student's *t*-test (ns, not significant; *, $P < 0.05$). See Supplementary Table S2 for MYC-sig gene signature information.

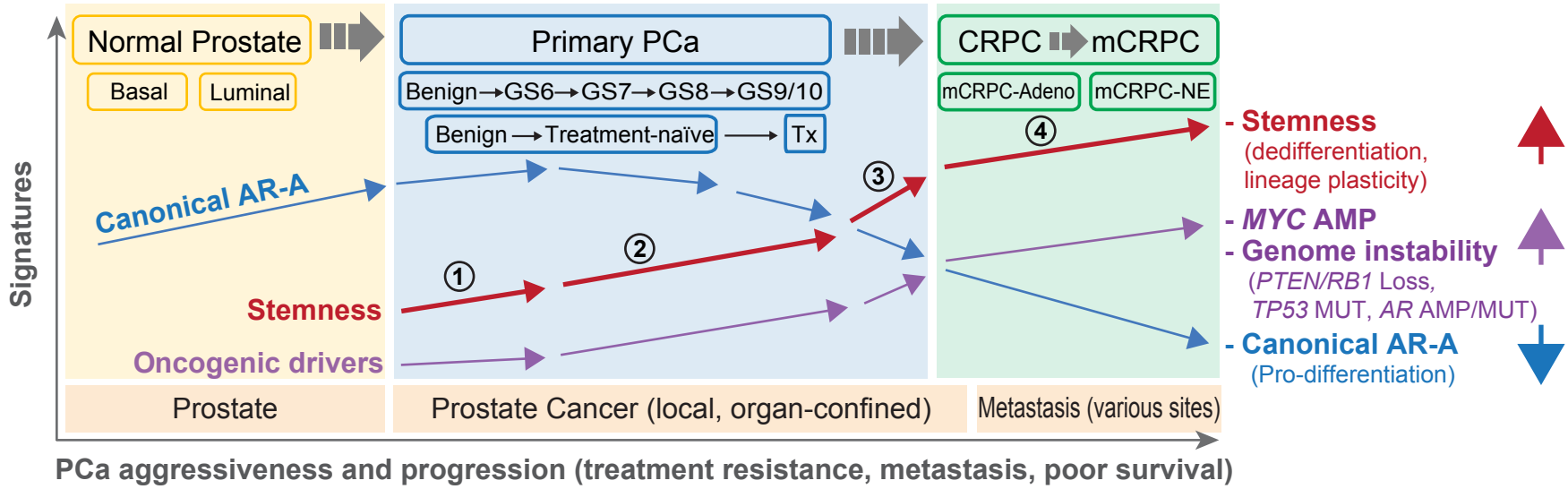

Supplementary Figure S10. Schematic summary of PCa progression and aggressiveness accompanied by gain of oncogenic Stemness and loss of prostatic epithelium differentiation defined by canonical AR signaling.

In the current study, we quantified the oncogenic dedifferentiation state (Stemness; indicated by red arrows) and canonical pro-differentiation AR signaling activity (AR-A; blue arrows) using transcriptomic data (3102 RNA-seq and 84081 microarray samples) collected from 26 datasets encompassing the evolutionary spectrum of PCa development and progression – normal prostate, early-stage and advanced primary tumors, metastatic castration-resistant PCa, and PCa subjected to long-term or neo-adjuvant androgen-deprivation therapy (ADT). Our analysis reveals a continual increase in the Stemness at all PCa progression stages, i.e., (1) PCa initiation and early tumor growth (compared with normal or matched benign prostate tissues); (2) natural tumor progression (treatment-naïve); and (3) long-term ADT to treatment resistance and metastasis. In contrast, the pro-differentiation AR-A displays a bell-shape trajectory with an increase in early-stage tumors followed by steady decreases in advanced tumors and the lowest in mCRPC. Our results also demonstrate that the increased AR-A represents a driving force of elevated Stemness in early PCa but tumor progression is accompanied by a divergence between decreasing AR-A and increasing Stemness, and clinical therapies such as ADT further diversify AR-A and Stemness. In fact, canonical AR-A shows an inverse correlation with the Stemness in treatment-failed mCRPC, and the Stemness tracks faithfully with the treatment-induced reprogramming. On the other hand, akin to the accompanying continually increasing Stemness, PCa progression is characterized by continually elevating *MYC* amplifications and activity, as well as increasing genome instability associated with deletion of tumor suppressors and *AR* amplifications and mutations (indicated by purple arrows). Importantly, high Stemness correlates with poor patient survival suggesting that Stemness is prognostic of patient outcomes, and increased Stemness represents a 'universal' feature of PCa progression and aggressiveness.